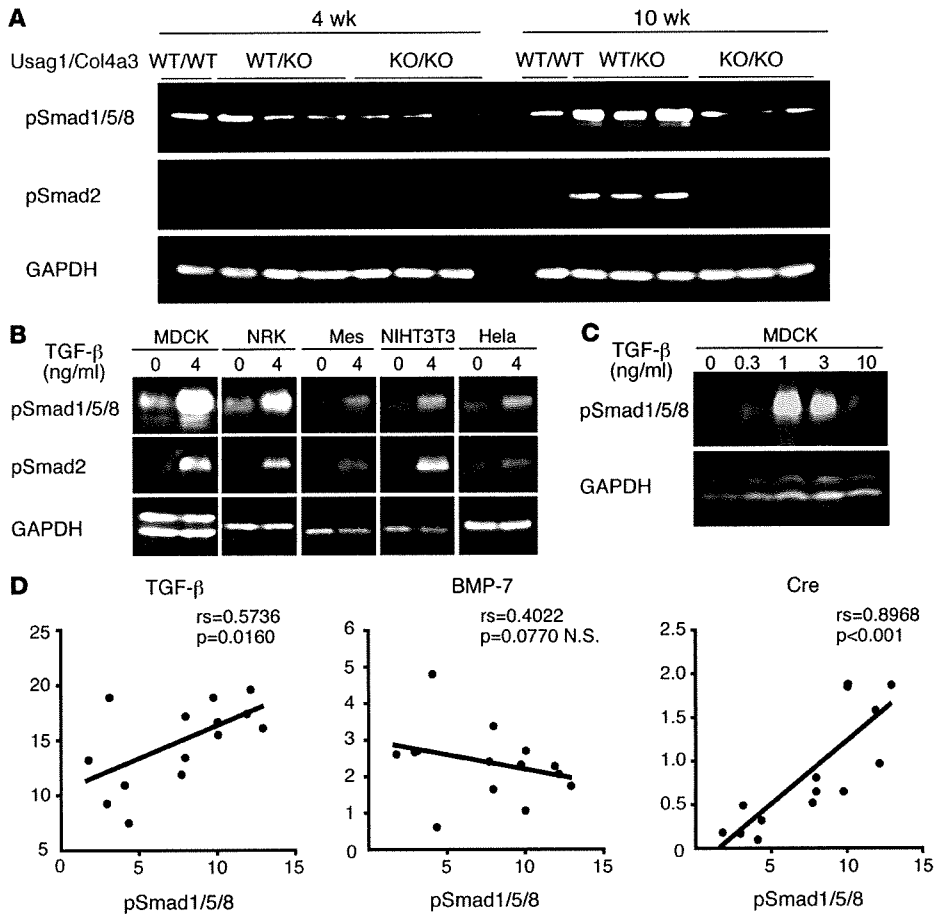

Figure 4
Smad1/5/8 phosphorylation was enhanced in *Usag1*$^{+/+}$*Col4a3*$^{-/-}$ mice, but not in *Usag1*$^{-/-}$*Col4a3*$^{-/-}$ mice. (**A**) Representative immunoblotting for Smad phosphorylation in the kidneys of WT littermates (WT/WT), *Usag1*$^{+/+}$ *Col4a3*$^{-/-}$ mice (WT/KO), and *Usag1*$^{-/-}$*Col4a3*$^{-/-}$ mice (KO/KO) at 4 and 10 weeks of ages. (**B**) A panel of cell lines were tested for the ability of TGF-β to induce phosphorylation of Smad1/5/8 in addition to Smad2. Cells were either left untreated or stimulated with 4 ng/ml of TGF-β for 1 hour. Whole-cell extracts were analyzed by immunoblotting using antibodies against phosphorylated Smad1/5/8 (pSmad1/5/8), pSmad2, and GAPDH as a loading control. (**C**) Representative immunoblotting showing the effect of various concentrations of TGF-β on the phosphorylation of Smad1/5/8 in MDCK cells. (**D**) Correlation between the phosphorylation levels of Smad1/5/8 in the kidneys of *Usag1*$^{+/+}$*Col4a3*$^{-/-}$ mice and mRNA expression of TGF-β and BMP-7 and serum creatinine (n = 14). The levels of phosphorylation of Smad1/5/8 were determined using the LAS image analysis system.

USAG-1 was not expressed in the Alport glomeruli. USAG-1 is expressed predominantly in the distal tubules, more specifically, in the thick ascending limb, distal convoluted tubules, and connecting tubules in adult kidneys, and not expressed in glomeruli (26). In situ hybridization was used to determine the expression of USAG-1 in *Usag1*$^{+/+}$*Col4a3*$^{-/-}$ mice and demonstrated that USAG-1 expression was not detectable in the glomeruli of *Usag1*$^{+/+}$*Col4a3*$^{-/-}$ mice either (Figure 6A) and was confined to tubules.

USAG-1 colocalizes with BMP-7 in the macula densa. Deficiency of USAG-1 significantly attenuated glomerular pathology in the *Col4a3*$^{-/-}$ mouse model of Alport syndrome in spite of the absence of USAG-1 expression in glomeruli. Further experiments focused on the part of the distal tubule that came in contact with its own glomerulus, the macula densa (Figure 6B). To determine whether USAG-1 is expressed in macula densa cells, we performed double staining of nNOS, a specific marker for macula densa, and β-gal using *Usag1*$^{+/LacZ}$ mice. As shown in Figure 6C, β-gal staining as well as immunostaining with anti-LacZ antibody colocalized with nNOS staining, indicating that USAG-1 was expressed in macula densa. BMP-7 is expressed in distal convoluted tubules, connecting tubules, collecting ducts, and podocytes (26). β-gal staining as well as immunostaining with anti-LacZ antibody also colocalized with nNOS in the kidneys of *Bmp7*$^{+/LacZ}$ mice, indicating the expression of BMP-7 in the macula densa (Figure 6C). Therefore, USAG-1 colocalizes with BMP-7 in the macula densa cells.

BMP-7 suppressed TGF-β–induced MMP-12 upregulation in mesangial cells, and USAG-1 antagonized the action of BMP-7. The macula densa, in which both USAG-1 and BMP-7 are expressed, is adjacent to mesangial cells in its own glomerulus (Figure 6B). To investigate potential mechanisms that are responsible for the beneficial effect of USAG-1 deficiency in Alport syndrome, the effect of BMP-7 and USAG-1 in cultured mesangial cells was examined. The expression of MMP-12 in cultured mesangial cells was upregulated by the administration of IL-1β and TGF-β, but not by the administration of MCP-1 (Figure 6D), in spite of the fact that MCP-1 is reported to stimulate MMP-12 expression in podocytes (29). The administration of BMP-7 suppressed TGF-β–induced MMP-12 upregulation in mesangial cells, and simultaneous administration of USAG-1 antagonized the suppressive effect of BMP-7 (Figure 6E). These results indicate that USAG-1 might enhance MMP-12 expression in the glomeruli by suppressing the inhibitory effect of BMP-7 and exacerbate glomerular disease progression in Alport syndrome.

Discussion

This study demonstrates that USAG-1 accelerates glomerular pathogenesis in a mouse model of human Alport syndrome, possibly through the crosstalk between the kidney tubules and its own glomerulus. *Usag1*$^{-/-}$*Col4a3*$^{-/-}$ mice demonstrated attenuated glomerular disease progression and preserved renal function in comparison with *Usag1*$^{+/+}$*Col4a3*$^{-/-}$ mice and significantly decreased

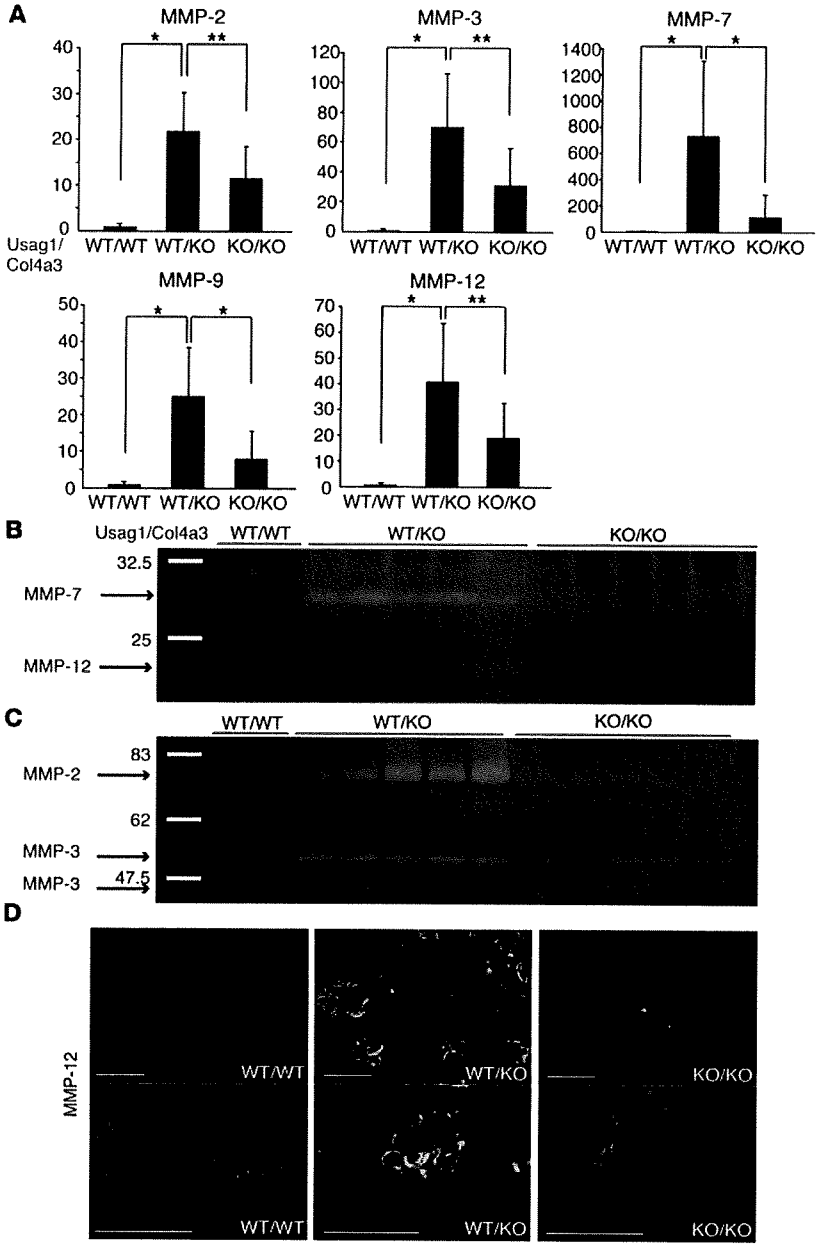

Figure 5

Usag1$^{-/-}$*Col4a3*$^{-/-}$ mice showed less expression and activity of MMPs in the kidneys. (**A**) Real-time RT-PCR analysis of MMP mRNA in the kidneys of WT littermates (WT/WT), *Usag1*$^{+/+}$*Col4a3*$^{-/-}$ mice, (WT/KO) and *Usag1*$^{-/-}$ *Col4a3*$^{-/-}$ mice (KO/KO) at 10 weeks of age. The expression levels were normalized to that of GAPDH and expressed relative to that in WT littermates (n = 10). Bars indicate the mean ± SD. *P < 0.001; **P < 0.01. (**B**) Casein zymography analyzing the kidneys of WT littermates (WT/WT), *Usag1*$^{+/+}$*Col4a3*$^{-/-}$ mice (WT/KO), and *Usag1*$^{-/-}$ *Col4a3*$^{-/-}$ mice (KO/KO) at 10 weeks of age. (**C**) Gelatin zymography analyzing the kidneys of WT littermates (WT/WT), *Usag1*$^{+/+}$*Col4a3*$^{-/-}$ mice (WT/KO), and *Usag1*$^{-/-}$*Col4a3*$^{-/-}$ mice (KO/KO) at 10 weeks of age. (**D**) Representative immunostaining for MMP-12 in the kidneys of WT littermates (WT/WT), *Usag1*$^{+/+}$*Col4a3*$^{-/-}$ mice (WT/KO), and *Usag1*$^{-/-}$*Col4a3*$^{-/-}$ mice (KO/KO) at 10 weeks of age. Scale bars: 100 μm.

expression and activity of MMPs, which play key roles in disease progression of Alport syndrome. Furthermore, USAG-1 and BMP-7 colocalized in the macula densa, a part of the distal tubules in contact with its own glomerulus, and BMP-7 reduced MMP-12 expression in mesangial cells, which was antagonized by USAG-1.

USAG-1 exacerbates glomerular injuries as well as tubular interstitial fibrosis. Tubular damage and interstitial fibrosis are the final common pathways leading to end-stage renal disease (ESRD) (38, 39) irrespective of the nature of the initial renal injury, and the degree of tubular damage parallels the impairment of renal function (39). Severe tubulointerstitial fibrosis is observed following glomerular injury in *Col4a3*$^{-/-}$ mice, and this exacerbates renal function. Because *Usag1*$^{-/-}$ mice were resistant to tubulointerstitial fibrosis (27), this resistance might contribute at least in part to the preservation of renal function in *Usag1*$^{-/-}$*Col4a3*$^{-/-}$ mice. In addition, *Usag1*$^{-/-}$ *Col4a3*$^{-/-}$ mice showed preserved GBM with less albuminuria in the early stage when tubular injury has yet to appear. Therefore, *Usag1*$^{-/-}$*Col4a3*$^{-/-}$ mice were resistant to both glomerular and tubular injuries.

USAG-1 increases the expression of MMP in Col4a3$^{-/-}$ *mice.* The molecular mechanisms by which the altered GBM composition in Alport syndrome causes renal pathogenesis remain unclear. It is proposed that abnormal persistence of α1/α1/α2(IV) collagen network in the adult GBM is associated with increased susceptibility to proteolysis by proteases in Alport syndrome (3, 9) and pharmacological ablation of MMP activities, especially MMP-12, leads to a significant attenuation in Alport disease progression (29, 40). The expression and activities of MMPs were significantly upregulated in the kidneys of *Usag1*$^{+/+}$*Col4a3*$^{-/-}$ mice, which is consistent with previous reports, and they were suppressed in the kidneys of *Usag1*$^{-/-}$*Col4a3*$^{-/-}$ mice. The suppression of MMP activities probably contributed, at least in part, to slow glomerular pathogenesis in *Usag1*$^{-/-}$*Col4a3*$^{-/-}$ mice. In addition, the administration of BMP-7 decreased the expression of MMP-12 in cultured mesangial cells, and USAG-1 antagonized the action of BMP-7. Therefore, USAG-1 might increase the expression of MMP in glomeruli and accelerate GBM destruction in *Col4a3*$^{-/-}$ mice.

Other possible roles of USAG-1 and BMP-7 in glomerular pathogenesis in Col4a3$^{-/-}$ *mice.* In addition to the inhibitory effect on MMP expression, BMP-7 possibly inhibits the progression of glomerular pathogenesis in *Col4a3*$^{-/-}$ mice at multiple steps. BMP-7 reduces the damage in podocytes (20, 41, 42) and mesangial cells (43–45) and attenuates the expression of inflammatory cytokines (46) and

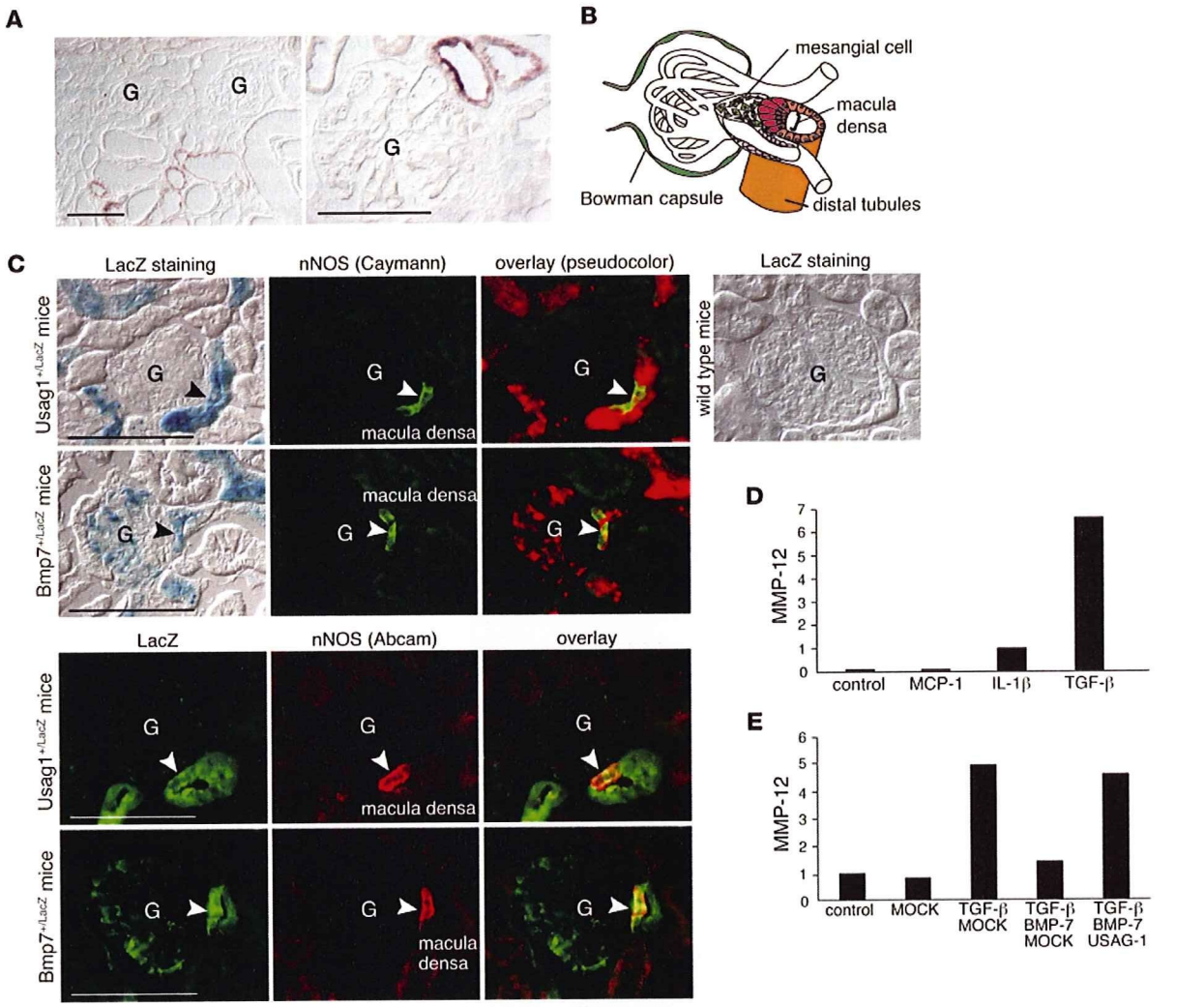

Figure 6

USAG-1 colocalizes with BMP-7 in the macula densa and inhibits the action of BMP-7 in mesangial cells. (**A**) In situ hybridization for USAG-1 mRNA in the kidneys of 10-week-old *Col4a3*$^{-/-}$ mice. Scale bars: 100 μm. G, glomerulus. (**B**) A schematic illustration of the juxtaglomerular apparatus. The macula densa is a part of distal tubules contacting with its glomerulus of origin and adjacent to mesangial cells. (**C**) β-Gal staining as well as immunostaining with anti-LacZ antibody colocalized with immunostaining with anti-nNOS (a marker for macula densa) antibody in the kidneys of *Usag1*$^{+/LacZ}$ mice and *Bmp7*$^{+/LacZ}$ mice. Kidney section from WT mice was also treated in the same way with the sections from *Usag1*$^{+/LacZ}$ mice and *Bmp7*$^{+/LacZ}$ mice and demonstrated no β-gal staining. Scale bars: 100 μm. (**D**) Real-time RT-PCR analysis of MMP-12 mRNA in cultured mesangial cells treated with inflammatory cytokines. The expression levels were normalized to those of GAPDH and expressed relative to those in controls. TGF-β markedly increased MMP-12 mRNA expression in mesangial cells. The graph reflects data that are representative for results of 4 independent experiments. (**E**) Real-time RT-PCR analysis of MMP-12 mRNA in cultured mesangial cells that were incubated with TGF-β, BMP-7, and USAG-1. BMP-7 suppressed TGF-β–induced MMP-12 upregulation in mesangial cells, and USAG-1 reversed the action of BMP-7. The graph reflects data that are representative for results of 4 independent experiments.

apoptosis in several types of cells (12, 41). Antagonizing the beneficial effects of BMP-7 by USAG-1 might enhance these injuries and accelerate glomerular pathogenesis in Alport syndrome.

USAG-1 secreted from distal tubules reaches the glomerulus and accelerates glomerular injury. Although the mechanism by which USAG-1 secreted from distal tubules reaches the glomerulus and exacerbates glomerular pathogenesis is not entirely clear, a crosstalk may exist between the distal tubule and the glomerulus in the same nephron.

The distal tubule of a nephron makes contact with the vascular pole of its glomerulus from which the distal tubule originated. At this point, there is a plaque of very specialized and differentiated cells in the distal tubule known as the macula densa (Figure 6B). The macula densa detects changes in the distal tubular fluid composition and transmits signals to the adjacent extraglomerular mesangial cells and afferent arterioles (47–53). Extraglomerular mesangial cells are anatomically in continuity with the glomerular mesangial cells and transmit the signal from the macula densa to the glomeru-

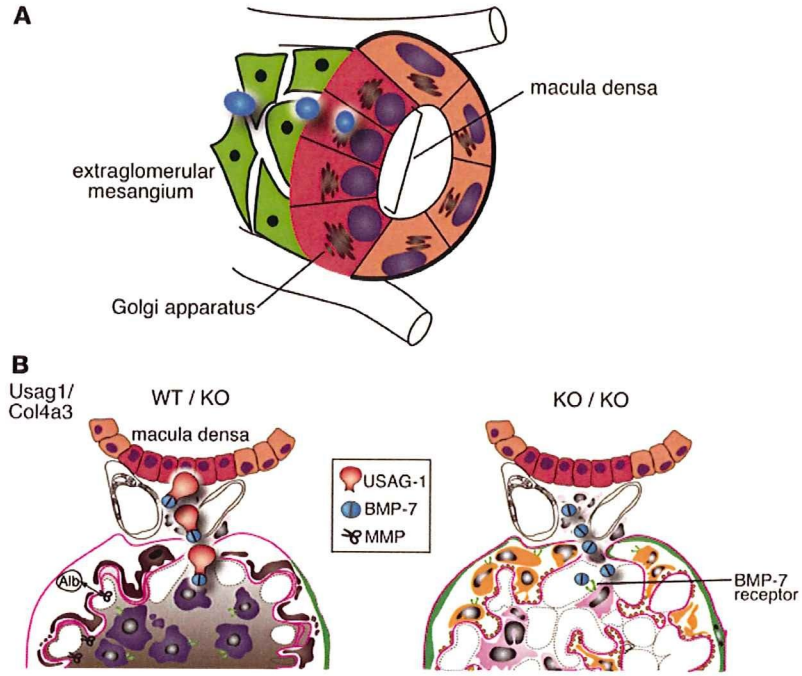

Figure 7
Hypothetical model for involvement of USAG-1 secreted from distal tubules in the pathogenesis of glomerular damage in Alport syndrome. (**A**) The macula densa (red), a part of the distal tubules, lies beside the extraglomerular mesangial cells (green), and the nuclei of the macula densa cells are apically located, suggesting the possibility that substances (blue) might be secreted from the basolateral membrane of the macula densa. Note that the basement membrane of the macula densa cells is continuous with the basement membrane of the extraglomerular mesangial cells. (**B**) In *Usag1*$^{+/+}$*Col4a3*$^{-/-}$ mice (WT/KO), the mesangial cells are activated (purple) and secrete MMPs (scissors), which degrade GBM. Following GBM destruction, podocytes residing on the GBM are damaged (brown) and albuminuria is observed. BMP-7 (blue) secreted from the macula densa is captured by USAG-1, which is also secreted from the macula densa. As a consequence, BMP-7 cannot bind to its receptors and exert its renoprotective action. In *Usag1*$^{-/-}$*Col4a3*$^{-/-}$ mice (KO/KO), BMP-7 secreted from the macula densa can bind to its receptors on mesangial cells and podocytes, and protect fragile alport GBM from degradation.

lus. The signals from the macula densa to the mesangial cells involve small diffusible substances (ATP or adenosine) released from the macula densa (47, 54). Multiphoton imaging demonstrates the water flow across the macula densa into the mesangial cell field at varying osmolarities in the luminal fluid (47). The histological characteristics of the macula densa also support the idea of substance transportation from the macula densa to mesangial cells: the nuclei of macula densa cells are apically located, while most of cell organelles tend to be located basally and laterally, thus indicating that the substances from the macula densa are possibly secreted basolaterally (Figure 7A). In addition, the basement membrane of the macula densa is fused with the basement membrane of the extraglomerular mesangial cells, indicating the lack of a barrier to interfere with the substance transportation from the macula densa to the glomerulus (Figure 7A). Furthermore, Hugo et al. demonstrated that extraglomerular mesangial cells function as reserve cells for glomerular mesangial cells (55). Extraglomerular mesangial cells stimulated by substances secreted from the macula densa migrate into glomerulus after glomerular injury and repopulate as mesangial cells.

As shown in Figure 6C, both USAG-1 and BMP-7 are expressed in the macula densa, and USAG-1 secreted from the basolateral membrane of macula densa could inhibit the action of BMP-7 on the adjacent mesangial cells. In the experiments using cultured mesangial cells, BMP-7 significantly attenuated TGF-β–induced MMP-12 upregulation, and the inhibitory effect of BMP-7 was abolished by the addition of USAG-1. Moreover, BMP-7 reduced TGF-β–induced cytotoxicity in mesangial cells (data not shown). Therefore, USAG-1 might exacerbate glomerular pathogenesis in Alport syndrome through accelerating upregulation of GBM-degrading enzyme and cytotoxicity by inhibiting the reno-protective effects of BMP-7 (Figure 7B).

An alternative possibility that may explain the effect of USAG-1 on glomerular injury is an interaction between circulating USAG-1 and BMP-7 in plasma. BMP-7 is present in plasma at a concentration range of 100–300 pg/ml (12). Due to the lack of an effective ELISA system, the plasma level of USAG-1 remains to be determined. If an appropriate amount of USAG-1 is present in the circulation, it could therefore bind to BMP-7 and thus inhibit its activity. To test the effect of circulating USAG-1 in the progression of *Col4a3*$^{-/-}$ mice, we performed systemic gene transfer of USAG-1 expression vector to *Usag1*$^{-/-}$*Col4a3*$^{-/-}$ mice and demonstrated that the difference in albuminuria between the gene transfer group and the control group was not statistically significant (Supplemental Figure 3).

Novel therapeutic approach for Alport syndrome. At present there is no definitive therapy to prevent or slow renal disease progression in Alport syndrome. Several studies using a mouse model of Alport syndrome have provided potential therapies, such as MMP inhibitor (29, 40), angiotensin-converting enzyme inhibitor (56), statins (57), transplantation of bone marrow–derived stem cells (58–60), and total body irradiation (61). The results of the present study support the notion that therapeutic trials to inhibit the function of USAG-1 may become a novel therapeutic approach for Alport syndrome either alone or in combination with other approaches. A therapeutic trial targeting USAG-1 is promising because it is expected to be effective in both glomerular and tubular injuries, is more kidney-specific, and has fewer extrarenal effects because the expression of USAG-1 is confined to the kidney.

Methods

Mice. The *Usag1*$^{-/-}$ mice used in this study have been described previously (27), and *Col4a3*$^{-/-}$ mice were purchased from Jackson Laboratory (JAX mice strain 129-Col4a3^{tm1Dec}/J) (62). *Usag1*$^{-/-}$*Col4a3*$^{-/-}$ mice were generated by breeding *Usag1*$^{+/-}$ and *Col4a3*$^{+/-}$ mice. *Col4a3*$^{-/-}$ littermates (*Usag1*$^{+/+}$*Col4a3*$^{-/-}$ mice) and WT littermates (*Usag1*$^{+/+}$*Col4a3*$^{+/+}$ mice) served as controls. All animal studies were approved by the Animal Research Committee, Graduate School of Medicine, Kyoto University, and performed in accordance with the guidelines of Kyoto University.

Age-matched mice were used for all studies. The ages of mice used in each experiment are described below.

Assessment of albuminuria. The mice were placed in metabolic cages, and urine was collected over a 24-hour period. During the urine collection, mice were allowed free access to food and water. Urinary albumin concentration was measured using the Albuwell M assay kit (Exocell).

Renal histopathology and electron microscopy. The kidneys were fixed in Carnoy's solution and embedded in paraffin. Sections (2-μm thick) were stained with PAS for routine histological examination, and the degree of morphological change was determined for ten 10-week-old mice and five 6-week-old mice per group by experienced pathologists who were blinded to the genotypes. The following parameters were evaluated: percentage of hemorrhagic glomeruli and sclerotic glomeruli; and tubular atrophy/interstitial fibrosis score. Tubular atrophy/interstitial fibrosis was graded as follows: grade 0, 0%–24%; grade 1, 25%–49%; grade 2, 50%–74%; grade 3, ≥ 75%.

Frozen sections of the kidneys were immunostained as previously described (63). The primary antibodies were against podocin (64), α1 (H11), and α3 (H31) chains of type IV collagen (a gift from Y. Sado; ref. 65), MCP-1 (R&D Systems), MMP-12 (Santa Cruz Biotechnology Inc.), nNOS (Cayman Chemical and Abcam), and LacZ (Cappel Laboratory). For double staining with β-gal, immunostaining was performed before β-gal staining to avoid the possibility that the deposition of X-gal might interfere with the antibody binding to the antigen. For electron microscopy, portions of the cortex were fixed in 2% glutaraldehyde and post-fixed in 1% osmic acid. After embedding, ultrathin sections were stained with uranyl acetate and lead citrate.

β-Gal staining and in situ hybridization. β-Gal staining and in situ hybridization were performed as described previously (26, 66). The probe for in situ hybridization of *USAG-1* mRNA contained the 1.0-kb open reading frame with GC content of 52.6%. Hybridization was detected using an anti-digoxigenin antibody conjugated with alkaline phosphatase and Nitro blue tetrazolium chloride/5-bromo-4-chloro-3-indolyl phosphate, 4-toluidine salt (Roche Diagnostics).

Immunoblotting. Whole-kidney tissue was homogenized in RIPA buffer and subjected to immunoblotting as previously described (67). The primary antibodies were anti-phospho-Smad1/5/8 (Cell Signaling Technology), phospho-Smad2 (Upstate Biotechnology), and GAPDH (Fitzgerald Industries).

Quantification of mRNA by real-time RT-PCR. Real-time RT-PCR was performed as described previously (27). Specific primers were designed using Primer Express software (Applied Biosystems). Serially diluted cDNA was used to generate the standard curve for each primer, and the PCR conditions were as follows: 50°C for 2 minutes, 95°C for 10 minutes, then 95°C for 15 seconds, and 60°C for 1 minute for 40 cycles.

Cell cultures. Mouse mesangial cells were established from glomeruli isolated from a 4-week-old normal mouse (C57BL/6J) and characterized as described previously (68). Cells of passage numbers 18 to 21 were cultured in DMEM/F12 containing 20% fetal calf serum.

Assessment of MMP mRNA expression in mesangial cells. Mesangial cells were seeded at a concentration of 5×10^4/ml. After 24 hours, the culture medium was replaced with DMEM containing 0.5% bovine serum albumin. The cells were incubated for 72 hours with 10 ng/ml MCP-1 (R&D Systems), 250 pg/ml IL-1β (R&D Systems), or 3 ng/ml TGF-β (R&D Systems) in the presence or absence of 20 ng/ml BMP-7 (R&D Systems) and then were analyzed for *MMP* mRNA expression by real-time RT-PCR. All experiments were performed in quadruplicate.

Production of recombinant USAG-1–Flag protein. A recombinant C-terminally Flag-tagged USAG-1 protein (USAG-1–Flag) was produced using the Baculovirus Expression System (Invitrogen) and purified from culture medium by affinity absorption on anti-FLAG M2 affinity beads (Sigma-Aldrich). Protein concentrations were estimated by Coomassie staining.

Zymography. Renal proteins were extracted as previously described (69). Samples standardized for protein concentration of 60 μg/lane were electrophoretically separated in 10% SDS-polyacrylamide gels that contained 1 mg/ml gelatin or α-casein. After separation, gels were placed in 2.5% Triton X-100 in PBS, washed, and incubated in developing buffer (50 mM Tris, pH 7.5, 200 mM NaCl, 5 mM CaCl2, and 0.02% Brij-35) overnight at 37°C. The gels were stained with 0.5% Coomassie blue R250 and then destained with a 10% acetic acid, 40% methanol solution until the gelatinolytic bands were clearly seen.

Systemic gene transfer. *Usag1*$^{-/-}$*Col4a3*$^{-/-}$ mice were injected with 300 μg of pcDNA3.1mUSAG-1 (cDNA for mouse USAG-1 cloned into the pcDNA3.1 expression vector) into the tibialis anterior muscle at 6 weeks as described (70) and were analyzed at 8 weeks for urinary albumin and renal histology.

Statistics. Data are presented as the mean ± SD. Statistical significance was assessed by Student's *t* test for 2 group comparisons and by ANOVA, followed by Fisher's protected least significant difference post-hoc test for multiple group comparisons. Significance was defined as a value of $P < 0.05$.

Acknowledgments

We thank Y. Kaziro, Y. Nabeshima, and T. Nakamura for valuable comments and discussion. We also thank Y. Sado for excellent subtype-specific antibodies against type IV collagen and J. Nakamura, N. Suzuki, and A. Hosotani for excellent technical assistance. This study was supported by grants-in-aid from the Ministry of Education, Culture, Science, Sports, and Technology of Japan (Wakate 177090551; Ho-ga 19659219; Kiban C 20590954), a grant-in-aid for Research on Biological Markers for New Drug Development, Health and Labour Sciences research grants from the Ministry of Health, Labor, and Welfare of Japan (08062855), a grant from the Astellas Foundation for Research on Metabolic Disorders, a grant from the Novartis Foundation for the promotion of science, a grant from the Kato Memorial Trust for Nambyo Research, a grant from the Hayashi Memorial Foundation for Female Natural Scientists, a grant from the Takeda Science Foundation, and a grant from the Japan Foundation for Applied Enzymology.

Received for publication November 24, 2009, and accepted December 16, 2009.

Address correspondence to: Motoko Yanagita, Career-Path Promotion Unit for Young Life Scientists, Kyoto University Graduate School of Medicine, Yoshida-konoe-cho, Sakyo-ku, Kyoto 606-8501, Japan. Phone: 81.75.753.9310; Fax: 81.75.753.9311; E-mail: motoy@kuhp.kyoto-u.ac.jp.

1. Kalluri R. Basement membranes: structure, assembly and role in tumour angiogenesis. *Nat Rev Cancer.* 2003;3(6):422–433.
2. Timpl R. Structure and biological activity of basement membrane proteins. *Eur J Biochem.* 1989;180(3):487–502.
3. Hudson BG, Tryggvason K, Sundaramoorthy M, Neilson EG. Alport's syndrome, Goodpasture's syndrome, and type IV collagen. *N Engl J Med.* 2003; 348(25):2543–2556.
4. Pescucci C, Longo I, Bruttini M, Mari F, Renieri A. Type-IV collagen related diseases. *J Nephrol.* 2003;16(2):314–316.
5. Barker DF, et al. Identification of mutations in the COL4A5 collagen gene in Alport syndrome. *Science.* 1990;248(4960):1224–1227.
6. Lemmink HH, et al. Mutations in the type IV collagen alpha 3 (COL4A3) gene in autosomal recessive Alport syndrome. *Hum Mol Genet.* 1994;3(8):1269–1273.
7. Mochizuki T, et al. Identification of mutations in the alpha 3(IV) and alpha 4(IV) collagen genes in autosomal recessive Alport syndrome. *Nat Genet.* 1994;8(1):77–81.
8. Zoja C, Morigi M, Benigni A, Remuzzi G. Genetics of rare diseases of the kidney: learning from mouse models. *Cytogenet Genome Res.* 2004;

105(2–4):479–484.
9. Kalluri R, Shield CF, Todd P, Hudson BG, Neilson EG. Isoform switching of type IV collagen is developmentally arrested in X-linked Alport syndrome leading to increased susceptibility of renal basement membranes to endoproteolysis. *J Clin Invest.* 1997;99(10):2470–2478.
10. Massague J, Chen YG. Controlling TGF-beta signaling. *Genes Dev.* 2000;14(6):627–644.
11. Helder MN, et al. Expression pattern of osteogenic protein-1 (bone morphogenetic protein-7) in human and mouse development. *J Histochem Cytochem.* 1995;43(10):1035–1044.
12. Vukicevic S, et al. Osteogenic protein-1 (bone morphogenetic protein-7) reduces severity of injury after ischemic acute renal failure in rat. *J Clin Invest.* 1998;102(1):202–214.
13. Zeisberg M, et al. Bone morphogenic protein-7 inhibits progression of chronic renal fibrosis associated with two genetic mouse models. *Am J Physiol Renal Physiol.* 2003;285(6):F1060–F1067.
14. Zeisberg M, et al. BMP-7 counteracts TGF-beta1-induced epithelial-to-mesenchymal transition and reverses chronic renal injury. *Nat Med.* 2003;9(7):964–968.
15. Morrissey J, Hruska K, Guo G, Wang S, Chen Q, Klahr S. Bone morphogenetic protein-7 improves renal fibrosis and accelerates the return of renal function. *J Am Soc Nephrol.* 2002;13(Suppl 1):S14–S21.
16. Hruska KA. Treatment of chronic tubulointerstitial disease: a new concept. *Kidney Int.* 2002; 61(5):1911–1922.
17. Hruska KA, Guo G, Wozniak M, Martin D, Miller S, Liapis H, Loveday K, Klahr S, Sampath TK, Morrissey J. Osteogenic protein-1 prevents renal fibrogenesis associated with ureteral obstruction. *Am J Physiol Renal Physiol.* 2000;279(1):F130–F143.
18. Hruska KA, Saab G, Chaudhary LR, Quinn CO, Lund RJ, Surendran K. Kidney-bone, bone-kidney, and cell-cell communications in renal osteodystrophy. *Semin Nephrol.* 2004;24(1):25–38.
19. Zeisberg M, Shah AA, Kalluri R. Bone morphogenic protein-7 induces mesenchymal to epithelial transition in adult renal fibroblasts and facilitates regeneration of injured kidney. *J Biol Chem.* 2005;280(9):8094–8100.
20. Wang S, de Caestecker M, Kopp J, Mitu G, Lapage J, Hirschberg R. Renal bone morphogenetic protein-7 protects against diabetic nephropathy. *J Am Soc Nephrol.* 2006;17(9):2504–2512.
21. Reddi AH. Interplay between bone morphogenetic proteins and cognate binding proteins in bone and cartilage development: noggin, chordin and DAN. *Arthritis Res.* 2001;3(1):1–5.
22. Yanagita M. BMP antagonists: Their roles in development and involvement in pathophysiology. *Cytokine Growth Factor Rev.* 2005;16(3):309–317.
23. Yanagita M. Modulator of bone morphogenetic protein activity in the progression of kidney diseases. *Kidney Int.* 2006; 70(6):989–993.
24. Eddy AA. Ramping up endogenous defences against chronic kidney disease. *Nephrol Dial Transplant.* 2006;21(5):1174–1177.
25. Yanagita M, et al. USAG-1: a bone morphogenetic protein antagonist abundantly expressed in the kidney. *Biochem Biophys Res Commun.* 2004; 316(2):490–500.
26. Tanaka M, et al. Expression of BMP-7 and USAG-1 (a BMP antagonist) in kidney development and injury. *Kidney Int.* 2008;73(2):181–191.
27. Yanagita M, et al. Uterine sensitization-associated gene-1 (USAG-1), a novel BMP antagonist expressed in the kidney, accelerates tubular injury. *J Clin Invest.* 2006;116(1):70–79.
28. Sayers R, Kalluri R, Rodgers KD, Shield CF, Meehan DT, Cosgrove D. Role for transforming growth factor-beta1 in alport renal disease progression. *Kidney Int.* 1999;56(5):1662–1673.
29. Rao VH, et al. Role for macrophage metalloelastase in glomerular basement membrane damage associated with alport syndrome. *Am J Pathol.* 2006;169(1):32–46.
30. Schmierer B, Hill CS. TGFbeta-SMAD signal transduction: molecular specificity and functional flexibility. *Nat Rev Mol Cell Biol.* 2007;8(12):970–982.
31. Wang SN, Lapage J, Hirschberg R. Loss of tubular bone morphogenetic protein-7 in diabetic nephropathy. *J Am Soc Nephrol.* 2001;12(11):2392–2399.
32. Daly AC, Randall RA, Hill CS. Transforming growth factor beta-induced Smad1/5 phosphorylation in epithelial cells is mediated by novel receptor complexes and is essential for anchorage-independent growth. *Mol Cell Biol.* 2008;28(22):6889–6902.
33. Goumans MJ, et al. Activin receptor-like kinase (ALK)1 is an antagonistic mediator of lateral TGFbeta/ALK5 signaling. *Mol Cell.* 2003;12(4):817–828.
34. Pannu J, Nakerakanti S, Smith E, ten Dijke P, Trojanowska M. Transforming growth factor-beta receptor type I-dependent fibrogenic gene program is mediated via activation of Smad1 and ERK1/2 pathways. *J Biol Chem.* 2007;282(14):10405–10413.
35. Kim JH, Ryu KH, Jung KW, Han CK, Kwak WJ, Cho YB. SKI306X suppresses cartilage destruction and inhibits the production of matrix metalloproteinase in rabbit joint cartilage explant culture. *J Pharmacol Sci.* 2005;98(3):298–306.
36. Kaneko Y, et al. Macrophage metalloelastase as a major factor for glomerular injury in anti-glomerular basement membrane nephritis. *J Immunol.* 2003;170(6):3377–3385.
37. Vos CM, van Haastert ES, de Groot CJ, van der Valk P, de Vries HE. Matrix metalloproteinase-12 is expressed in phagocytotic macrophages in active multiple sclerosis lesions. *J Neuroimmunol.* 2003;138(1–2):106–114.
38. Eddy AA. Molecular insights into renal interstitial fibrosis. *J Am Soc Nephrol.* 1996;7(12):2495–2508.
39. van Kooten C, Daha MR, van Es LA. Tubular epithelial cells: A critical cell type in the regulation of renal inflammatory processes. *Exp Nephrol.* 1999;7(5–6):429–437.
40. Zeisberg M, et al. Stage-specific action of matrix metalloproteinases influences progressive hereditary kidney disease. *PLoS Med.* 2006;3(4):e100.
41. Mitu GM, Wang S, Hirschberg R. BMP7 is a podocyte survival factor and rescues podocytes from diabetic injury. *Am J Physiol Renal Physiol.* 2007;293(5):F1641–F1648.
42. De Petris L, Hruska KA, Chiechio S, Liapis H. Bone morphogenetic protein-7 delays podocyte injury due to high glucose. *Nephrol Dial Transplant.* 2007;22(12):3442–3450.
43. Otani H, et al. Antagonistic effects of bone morphogenetic protein-4 and -7 on renal mesangial cell proliferation induced by aldosterone through MAPK activation. *Am J Physiol Renal Physiol.* 2007;292(5):F1513–F1525.
44. Chan WL, Leung JC, Chan LY, Tam KY, Tang SC, Lai KN. BMP-7 protects mesangial cells from injury by polymeric IgA. *Kidney Int.* 2008;74(8):1026–1039.
45. Wang S, Hirschberg R. BMP7 antagonizes TGF-beta-dependent fibrogenesis in mesangial cells. *Am J Physiol Renal Physiol.* 2003;284(5):F1006–F1013.
46. Gould SE, Day M, Jones SS, Dorai H. BMP-7 regulates chemokine, cytokine, and hemodynamic gene expression in proximal tubule cells. *Kidney Int.* 2002;61(1):51–60.
47. Bell PD, Lapointe JY, Peti-Peterdi J. Macula densa cell signaling. *Annu Rev Physiol.* 2003;65:481–500.
48. Barajas L. Anatomy of the juxtaglomerular apparatus. *Am J Physiol.* 1979;237(5):F333–F343.
49. Lapointe JY, Laamarti A, Bell PD. Ionic transport in macula densa cells. *Kidney Int Suppl.* 1998; 67:S58–S64.
50. Navar LG, Inscho EW, Majid SA, Imig JD, Harrison-Bernard LM, Mitchell KD. Paracrine regulation of the renal microcirculation. *Physiol Rev.* 1996;76(2):425–536.
51. Navar LG, Ploth DW, Bell PD. Distal tubular feedback control of renal hemodynamics and autoregulation. *Annu Rev Physiol.* 1980;42:557–571.
52. Schnermann J, et al. Tubuloglomerular feedback: new concepts and developments. *Kidney Int Suppl.* 1998;67:S40–S45.
53. Tojo A, Onozato ML, Fujita T. Role of macula densa neuronal nitric oxide synthase in renal diseases. *Med Mol Morphol.* 2006;39(1):2–7.
54. Ren Y, Carretero OA, Garvin JL. Role of mesangial cells and gap junctions in tubuloglomerular feedback. *Kidney Int.* 2002;62(2):525–531.
55. Hugo C, Shankland SJ, Bowen-Pope DF, Couser WG, Johnson RJ. Extraglomerular origin of the mesangial cell after injury. A new role of the juxtaglomerular apparatus. *J Clin Invest.* 1997;100(4):786–794.
56. Gross O, et al. Preemptive ramipril therapy delays renal failure and reduces renal fibrosis in COL4A3-knockout mice with Alport syndrome. *Kidney Int.* 2003;63(2):438–446.
57. Koepke ML, Weber M, Schulze-Lohoff E, Beirowski B, Segerer S, Gross O. Nephroprotective effect of the HMG-CoA-reductase inhibitor cerivastatin in a mouse model of progressive renal fibrosis in Alport syndrome. *Nephrol Dial Transplant.* 2007;22(4):1062–1069.
58. Sugimoto H, Mundel TM, Sund M, Xie L, Cosgrove D, Kalluri R. Bone-marrow-derived stem cells repair basement membrane collagen defects and reverse genetic kidney disease. *Proc Natl Acad Sci U S A.* 2006;103(19):7321–7326.
59. Floege J, Kunter U, Weber M, Gross O. Bone marrow transplantation rescues Alport mice. *Nephrol Dial Transplant.* 2006;21(10):2721–2723.
60. Prodromidi EI, et al. Bone marrow-derived cells contribute to podocyte regeneration and amelioration of renal disease in a mouse model of Alport syndrome. *Stem Cells.* 2006;24(11):2448–2455.
61. Katayama K, et al. Irradiation prolongs survival of Alport mice. *J Am Soc Nephrol.* 2008;19(9):1692–1700.
62. Cosgrove D, et al. Collagen COL4A3 knockout: a mouse model for autosomal Alport syndrome. *Genes Dev.* 1996;10(23):2981–2992.
63. Yanagita M, et al. Gas6 regulates mesangial cell proliferation through Axl in experimental glomerulonephritis. *Am J Pathol.* 2001;158(4):1423–1432.
64. Kawachi H, Koike H, Kurihara H, Sakai T, Shimizu F. Cloning of rat homologue of podocin: expression in proteinuric states and in developing glomeruli. *J Am Soc Nephrol.* 2003;14(1):46–56.
65. Sado Y, et al. Establishment by the rat lymph node method of epitope-defined monoclonal antibodies recognizing the six different alpha chains of human type IV collagen. *Histochem Cell Biol.* 1995;104(4):267–275.
66. Valenzuela DM, et al. High-throughput engineering of the mouse genome coupled with high-resolution expression analysis. *Nat Biotechnol.* 2003;21(6):652–659.
67. Yanagita M, et al. Gas6 induces mesangial cell proliferation via latent transcription factor STAT3. *J Biol Chem.* 2001;276(45):42364–42369.
68. MacKay K, Striker LJ, Elliot S, Pinkert CA, Brinster RL, Striker GE. Glomerular epithelial, mesangial, and endothelial cell lines from transgenic mice. *Kidney Int.* 1988;33(3):677–684.
69. Rodgers KD, et al. Monocytes may promote myofibroblast accumulation and apoptosis in Alport renal fibrosis. *Kidney Int.* 2003;63(4):1338–1355.
70. Lories RJ, Derese I, Luyten FP. Modulation of bone morphogenetic protein signaling inhibits the onset and progression of ankylosing enthesitis. *J Clin Invest.* 2005;115(6):1571–1579.

LETTERS TO THE EDITOR

Successful treatment of membranoproliferative glomerulonephritis associated with hepatitis B and C virus simultaneous infection patient

A. Mima[1,2], N. Iehara[2], T. Matsubara[2], S. Yamamoto[2], H. Abe[1], K. Nagai[1], M. Matsuura[1], T. Murakami[1], S. Kishi[1], T. Araoka[1], F. Kishi[1], N. Kondo[1], R. Shigeta[1], K. Yoshikawa[1], T. Takahashi[1], T. Kita[3], T. Doi[1] and A. Fukatsu[2]

[1]Department of Nephrology, Institute of Health Biosciences, The University of Tokushima Graduate School, Tokushima, [2]Departments of Nephrology and [3]Cardiovascular Medicine, Kyoto University Graduate School of Medicine, Kyoto, Japan

Sir, – More and more epidemiological evidence suggests that hepatitis B virus (HBV) and hepatitis C virus (HCV) are associated with glomerular disease, the foremost being membranoproliferative glomerulonephritis (MPGN) [1].

Several histological findings have been reported in renal biopsies obtained from patients with glomerulonephritis including MPGN associated with chronic HBV infection, although the pathogenesis of hepatitis B glomerulonephritis remains unknown.

Administration of interferon-α and ribavirin are currently used in the treatment of MPGN associated with HCV [2], while only in few patients treatment of HBV related MPGN with interferon has been described. Moreover, there is even less evidence of treatment of MPGN associated with simultaneous HBV and HCV infection. Here, we report a case of proteinuria due to MPGN associated with simultaneous HBV and HCV infection.

A 62-year-old woman presented with edema of legs since 10 months and hypertension. Her significant medical history was a thoracoplasty due to tuberculosis with blood transfusion 44 years ago. At admission physical examination showed hypertension (160/90 mmHg). The liver and spleen were not palpable. She did not show any abnormalities in the neurologic tests. The laboratory findings were hemoglobin 10.4 g/dl, blood urea nitrogen (BUN) 23 mg/dl, creatinine 1.1 mg/dl with a creatinine clearance of 61 ml/min, total serum proteins 6.7 g/dl, albumin 3.9 g/dl, cholesterol 175 mg/dl, asparate aminotransferase 36 U/l, alanine aminotransferase 24 U/l, alkaline phosphatase 151 U/l, lactate dehydrogenase 266 U/l. Serological work-up showed C3 75.7 mg/dl, C4 8.9 mg/dl, and CH50 of < 7.0 U/ml. Immunoglobulins: IgG 1,592 mg/dl, IgA 151 mg/dl, IgM 139 mg/dl. Other serological data were normal or negative including CRP, ANA, double-strand DNA, ABGM, MPO- and PR3-ANCA. Cryoglobulinemia was found along with positive rheumatoid factor (35.6 IU/ml). Virologic studies were positive for HBs antigen and HBc and HBe antibody. HBV DNA and HCV RNA in serum were detected by quantitative polymerase chain reaction assay. The HBV DNA titer was 4.5 Log copy/ml. The HCV genotype was group Ib and HCV RNA titer showed 1,680 KU/ml. Urine examination revealed 3+ proteinuria and 24-h urinary protein was 2.2 g. On the fifth admission day, renal biopsy was performed. A specimen evaluated with light microscopy showed 2 of 14 glomeruli sclerosed. The glomeruli had diffuse hypercellularity with a marked increase in mesangial cells and matrix, resulting in an appearance of lobular formation. The glomerular capillary loops were thickened and double contours were recognized. There were no periodic acid-Schiff's (PAS)-positive deposits. Immunofluorescence analysis revealed granular capillary wall and mesangial regions staining that was predominantly for IgG with little IgM or C3. IgA and C1q were negative. These features were consistent with type I MPGN associated with HBV and HCV infection. A liver biopsy was not performed but there was no evidence of cirrhosis on ultrasound examination of the abdomen. Blood pressure control was poor despite treatment cilnidipine 20 mg once a day and amlodipine besilate 5 mg once a day. To reduce proteinuria and high blood pressure, olmesartan 40 mg once a day was initiated. In July 2006, therapy with interferon-α 40 μg per week and

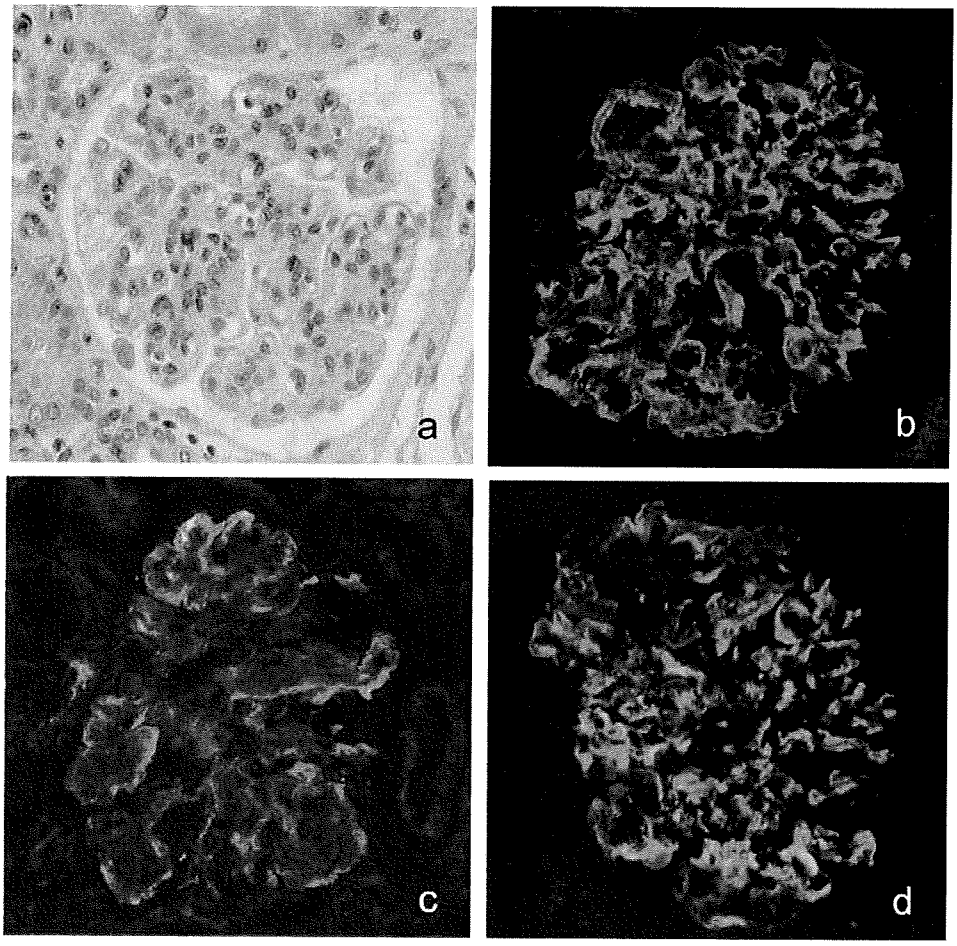

Figure 1. Light microscopic: Proliferation of endocapillary cells and mesangial cells as well as matrix are visible, resulting in a lobular formation appearance. (a) Periodic acid-Schiff stain. Original magnification × 400. Immunofluorescence microscopy, using polyclonal IgG antibodies, showing deposits only in the mesangium; these deposits were graded on a scale of 0 to 4+ as 3+ for IgG (b), 2+ for IgM (c), and 3+ for C3 (d). Original magnification × 400.

rivabirin 400 mg per day was started. After 6 weeks, despite the initially good clinical response, hemolytic anemia appeared and rivabirin was tapered off. 4 weeks later, anemia had improved and rivabirin was started again. We increased rivabirin to a dose of 800 mg/day 4 weeks after restarting rivabirin. In December 2006, the patient showed no appearance of HBV-DNA and HCV-RNA by quantitative blood analysis. One year after treatment, the patient was still in clinical and virologic remission.

This case suggests that the association of MPGN with chronic hepatitis is due to replicative HBV and HCV. The HCV associated CGN seems to be related to the glomerular deposition of immune complexes made by the HCV antigen, anti-HCV IgG antibodies, and a rheumatoid factor, which is an IgM kappa [3], while several studies reveal that patients with MPGN have a significant HBsAg carrier rate and report the pathogenesis to be immune complex mediated [4], though glomerular deposits of HBsAg may not be detectable as in our present case. The cause and effect relationship of HBV infection and glomerulonephritis could be proven only by demonstrating disappearance of the glomerular abnormalities on histology following seroconversion of virus after interferon therapy. In our case, HBV DNA had disappeared and clinical remission was prominent though seroconversion of HBV had not been achieved. Recently, it has been reported that interferon in HBV-associated glomerulonephritis achieved remission of proteinuria without seroconversion to anti-HBe [5]. The mechanism of remission of proteinuria using interferon in simultaneous

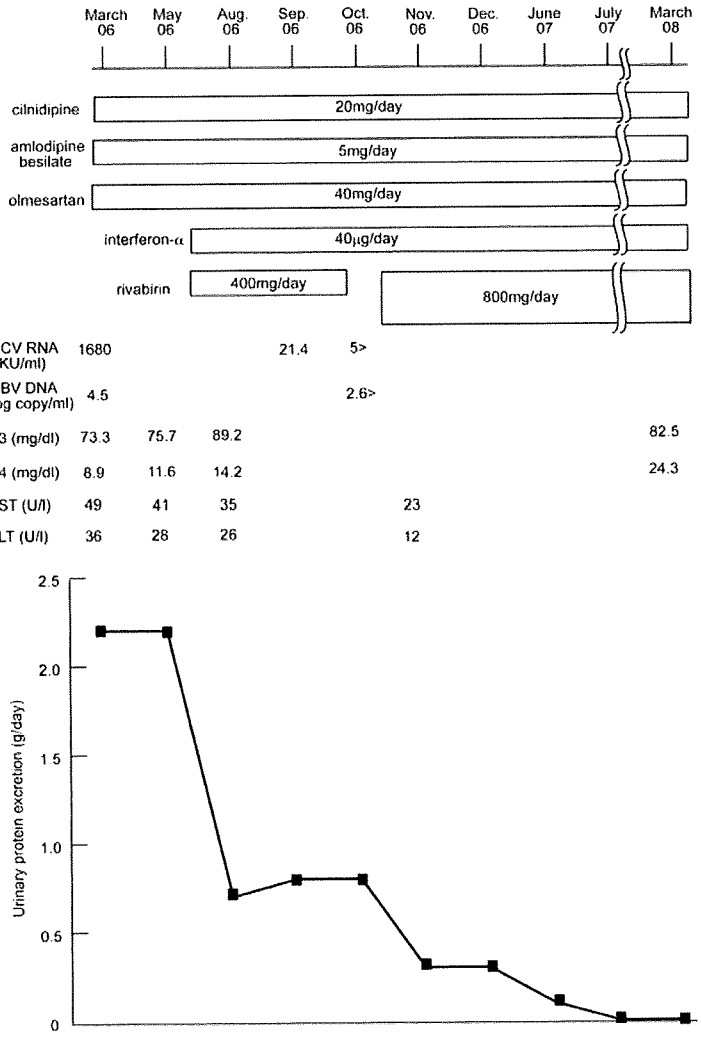

Figure 2. Clinical course of the patient.

HBV and HCV related glomerulonephritis is still unclear and requires further study.

Regarding treatment of HCV related glomerulonephritis, a combined therapy with interferon-α and ribavirin has become the standard treatment [6]. Once this combination therapy was started in our case, proteinuria and viremia were further decreased. Proteinuria dropped to a minimum level of 200mg per day 8 weeks after starting this therapy. HCV RNA titers were also significantly reduced. Owing to hemolytic anemia, ribavirin was stopped for a little while. Karmar et al. recommend to treat HCV related glomerulonephritis patients for at least 48 weeks and to continue the anti-viral therapy even in the absence of a decrease in HCV RNA concentration of 2 log at week 12 [7]. This is why we are now still continuing anti-viral therapy.

The present case demonstrated a patient with MPGN associated with simultaneous HBV and HCV infection. She achieved clinical remission under a full spectrum of drugs. We conclude that MPGN can be associated with simultaneous HBV and HCV infection and responds well to therapy with interferon-α and ribavirin.

References

[1] *Johnson RJ, Willson R, Yamabe H, Couser W, Alpers CE, Wener MH et al.* Renal manifestations of hepatitis C virus infection. Kidney Int. 1994; *46:* 1255-1263.

[2] *Johnson RJ, Gretch DR, Couser WG, Alpers CE, Wilson J, Chung M et al.* Hepatitis C virus-associated glomerulonephritis. Effect of alpha-interferon therapy. Kidney Int. 1994; *46:* 1700-1704.

[3] *Johnson RJ, Gretch DR, Yamabe H, Hart J, Bacchi CE, Hartwell P et al.* Membranoproliferative glomerulonephritis associated with hepatitis C virus infection. N Engl J Med. 1993; *328:* 465-470.

[4] *Johnson RJ, Couser WG.* Hepatitis B infection and renal disease: clinical, immunopathogenetic and therapeutic considerations. Kidney Int. 1990; *37:* 663-676.

[5] *Chung DR, Yang WS, Kim SB, Yu E, Chung YH, Lee Y et al.* Treatment of hepatitis B virus associated glomerulonephritis with recombinant human alpha interferon. Am J Nephrol. 1997; *17:* 112-117.

[6] *Alric L, Plaisier E, Thebault S, Peron JM, Rostaing L, Pourrat J et al.* Influence of antiviral therapy in hepatitis C virus-associated cryoglobulinemic MPGN. Am J Kidney Dis. 2004; *43:* 617-23.

[7] *Kamar N, Boulestin A, Selves J, Esposito L, Sandres-Saune K, Stebenet M et al.* Factors accelerating liver fibrosis progression in renal transplant patients receiving ribavirin monotherapy for chronic hepatitis C. J Med Virol. 2005; *76:* 61-68.

A. Mima, MD, PhD
Department of Nephrology
Institute of Health Biosciences
The University of Tokushima Graduate School
Tokushima 770-8503, Japan
akiramima@clin.med.tokushima-u.ac.jp

【腎障害・壊死におけるシグナル伝達】

抗生物質と細胞毒*

市村隆治**　増田智先***

はじめに：細胞毒による尿細管上皮細胞の損傷と細胞死

急性腎障害において，虚血と細胞毒は重要な尿細管上皮細胞の損傷，細胞死の原因であり，その発症メカニズムにおける細胞内シグナリングの役割を理解することはきわめて重要と考えられる。同時に，尿細管上皮細胞の損傷や細胞死に対する防御方法をさぐることもできる。

抗生物質や細胞毒，さらには虚血による腎障害では，それらの刺激に特に感受性の強い近位尿細管上皮細胞が標的となる。そこで，抗生物質とそのほかの腎特異的な細胞毒による近位尿細管上皮細胞の損傷メカニズムを理解するためには，細胞の普遍的な損傷のメカニズムと近位尿細管上皮細胞の分化機能（特に毒物の分布，濃縮）に関係した損傷メカニズムの両方を考慮しなければならない。本稿でとりあげる抗生物質と細胞毒による毒性は近位尿細管上皮細胞内に濃縮されることによって発現するということからも明らかであろう。

腎毒性の重要な原因となる，抗生物質とそのほかの細胞毒として抗癌薬であるシスプラチンをとりあげて，これらの物質の腎毒性発現における細胞内シグナリングの役割を検討したい。

また，われわれの研究成果を例としてシグナリングを利用した細胞毒性への防御のメカニズムについて述べる。

Ⅰ．毒物と細胞死―細胞死には細胞内シグナリングの役割をもつ

細胞の生存，恒常性（ホメオスタシス）の維持，そして細胞死において，細胞内シグナリングはきわめて重要な役割を果たしている。細胞の生死は，生命維持と細胞死という側面の細胞内シグナリングのバランスによって成り立っている[1]。近位尿細管上皮細胞のように分化して特異的な働きをしている細胞であれば，その分化と機能の恒常性の維持もまた細胞内シグナリングによって調節されている。一般に理解されている細胞毒性のメカニズムは，この細胞内オルガネラの破壊（DNA やミトコンドリアの損傷など）によってもたらされる細胞のバランス機能の攪乱によるものである。この毒性メカニズムを理解するうえで大切なことは，毒物によってどの細胞内シグナリング，パスウェイが標的となって，またどのような形で攪乱されているのかということである。このように「恒常性」は，以下に述べるように細胞死シグナリングの抑制，または促進などといった細胞の生死を支

---

* Antibiotics and nephrotoxicants

key words：アポトーシス，ネクローシス，オートファジー，小胞体ストレス，ゲンタマイシン，シスプラチン

** Renal Division, Department of Medicine, Brigham and Women's Hospital, Harvard Medical School
ICHIMURA Takaharu
〔4 Blackfan Circle, Boston, MA 02115, USA〕
*** 京都大学医学部附属病院薬剤部　MASUDA Satohiro

配する重要な機能を含んでいる。したがって，細胞毒性の発現という細胞の損傷と死を招く深刻な刺激下において，生存シグナリングによる調節メカニズムは細胞毒に対する主要な応答機能と考えられる[2]。すなわち，細胞毒性発現の分子メカニズムや，それを阻止するための方法論を見出すには，細胞内で営まれるシグナリングの理解が大切である。

近年のトキシコゲノミクスやプロテオミクスといった研究も，未知の毒性の標的や毒性への応答を見出すための網羅的探索法として行われている。

II．細胞死のタイプ，メカニズムと細胞内シグナリング

最近の研究によって[3]，いずれのタイプの細胞死もプログラム細胞死であることがわかってきている。プログラム細胞死とは死のプロセスが細胞内のメカニズムによって制御されていて，単純なシステムの破綻ではないことをいう。ここで細胞死のタイプとその細胞内シグナリング，毒性の標的や毒性への応答に重要ないくつかの細胞内シグナリングメカニズムを簡単に紹介する。

1．アポトーシス（図1）

最も代表的なプログラム細胞死であり，染色体DNAの断片化によって特徴づけられる。アポトーシスはホメオスタシスの一部であり正常な組織や発生の途上で常に起こっているが，毒性作用によっても誘導される[1,3]。デスリガンドとデスリセプター（受容体）を介した外因性のアポトーシスと内因性のシグナルによるアポトーシスの2つのタイプがある。

主に内因性のアポトーシスによる細胞内シグナリングメカニズムを簡単に説明する。さまざまな細胞ストレスが原因となってアポトーシスの引き金（トリガー）となる因子の活性化が起こる。

p53はアポトーシスのトリガー因子の代表とされており，活性化されたこれらの刺激がBcl2ファミリーの蛋白質を活性化する。特にBax，Bad，Bakなどのアポトーシスを促進させる蛋白質が，このシグナリング経路で重要な役割を担うミトコンドリアを刺激する。Bcl2や$BcLX_L$はこれを阻害する作用をもつ。ミトコンドリアの刺激によって，チトクロムCやOmi，Smacなどアポトーシスシグナルを促す重要な蛋白質の漏出が誘導される。漏出されたチトクロムCはカスパーゼ9，そして染色体DNAや細胞内蛋白質の断片化を媒介するカスパーゼ3と7の活性化によるアポトーシスを引き起こす。OmiやSmacはカスパーゼ活性化の促進という役割を担う。細胞の生命維持にとって，このアポトーシスシグナルの抑制が重要であり，いくつかの抑制機構が知られている。Bcl2などの阻害因子は最もよく知られているが，そのほか蛋白質リン酸化酵素でありMAPキナーゼファミリーに属するERKはアポトーシスを抑制する機能を有する[4]。一方，同じMAPキナーゼでも，JNKやp38はアポトーシスを促進する作用がある。また，PI3KやAKTもアポトーシスを抑制する。

2．ネクローシス

細胞内小器官の膨化によって特徴づけられる。従来，制御不能な細胞死と理解されてきたが，ネクローシスもまたプログラム細胞死の1つとして最近理解されつつある[3,5]。病理学的には，ヒトや実験動物の虚血または腎毒性による急性腎障害（AKI）において，このタイプの細胞死が死んだ近位尿細管上皮細胞の比較的多数を占めている。ネクローシスにおいても，ミトコンドリアの役割が重要であり，ERKはネクローシスの抑制作用も有する[6]。

3．小胞体ストレスによる細胞死

小胞体ストレス自体はストレス応答の機構であるが，細胞毒が小胞体を標的としている場合，細胞死を誘導するシグナルが小胞体から送られ細胞死（アポトーシス，ネクローシス）を誘導することがある[7]。この一連の反応は，小胞体ストレスシグナリング経路によって制御されている。小胞体ストレスはミトコンドリア機能と深くかかわっ

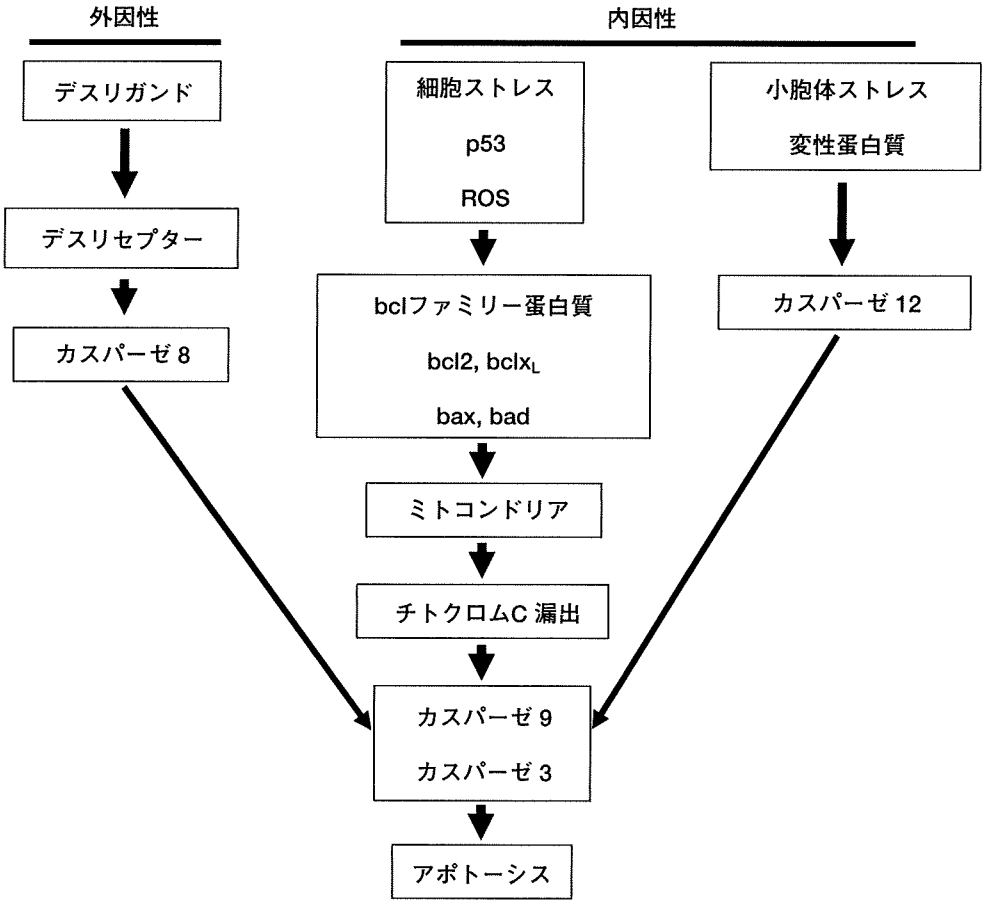

図1　アポトーシスシグナル伝達経路

ており，Bcl2 ファミリーの蛋白質の活性化による小胞体ストレスの誘導，引き続くカスパーゼ 12 そしてカスパーゼ 3 の活性化，さらに，小胞体ストレスシグナリングを制御する IRE1a への Bax や Bak の結合による JNK シグナル経路の活性化や，ほかの小胞体ストレス制御因子による転写因子 gadd153/CHOP10 の活性化などを介して細胞死を誘導する。

4．オートファジーによる細胞死

オートファジーは，アミノ酸の供給・再利用を重要な役割としており，ミトコンドリアなど細胞内器官の自食作用のために形成されるオートファーゴソームを特徴とする[3]。オートファジー自体は飢餓ストレスに対する応答機構であるが，細胞死を誘導する場合がある。最近の知見では，オートファジーはシスプラチンの腎毒性に対し防御作用があるといわれている[8,9]。

III．腎毒性のある抗生物質と毒物

腎毒性と細胞毒性による細胞死シグナリングについて，2 つの細胞毒を例にとって述べよう（**図 2**）。まず腎毒性に特徴的なことは，近位尿細管上皮細胞の機能，すなわち細胞毒の濃縮的な細胞内蓄積，代謝，尿細管分泌，再吸収といったことである。腎毒性作用の場合，上皮細胞は細胞毒を濃縮することと，ミトコンドリアにおけるエネルギー代謝が活発なために毒性作用に対して感受性が高いことがあげられる[1]。こうした腎上皮細胞の分化した特徴と細胞死シグナリングは関係してくる。ここでは主に培養細胞を用いた研究成果からの知見をまとめる。

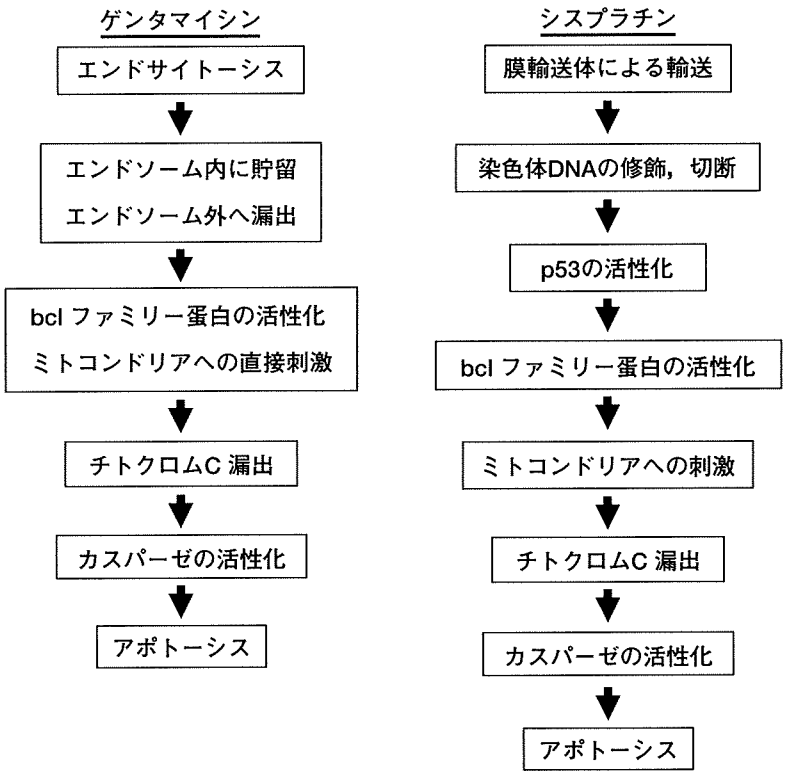

図2　ゲンタマイシンとシスプラチンの毒性シグナル伝達経路

1．ゲンタマイシン

エンドソームの飽和，ミトコンドリアの刺激と活性酸素の発生

ゲンタマイシンは近位尿細管上皮細胞の絨毛に発現している受容体メガリン（gp330）に結合し，エンドサイトーシスを介して細胞内に取り込まれ，エンドソームに蓄積される[1]。最終的にここから細胞質に流出されることによって毒性を惹起し，Bax の活性化，ミトコンドリアからのシトクロム C 漏出を経て，アポトーシスシグナリングを発生させる。またゲンタマイシンは細胞内の活性酸素生成も引き起こし，この経路からも細胞死に寄与している。

2．シスプラチン

DNA 損傷と p53 の活性化

シスプラチンは近位尿細管上皮細胞上の有機カチオントランスポータ（OCT2/SLC22A2）によって細胞内に取り込まれ，核内の染色体 DNA と共有結合し，最終的に DNA の切断を惹起する[10~12]。この DNA 損傷が p53 の活性化を誘導し，PUMA，PIDD といったアポトーシス促進因子の転写の誘導につながり，または直接 Bcl ファミリー蛋白質の活性化を引き起こして，ミトコンドリアの刺激，シトクロム C の漏出を介して，アポトーシスシグナリングの発生へと進行する。このメカニズムは，シスプラチンの抗癌薬としての作用と類似している[12]。シスプラチンの毒性には MAP キナーゼの活性化も重要な役割をもつ。JNK，p38 とともに通常は抗アポトーシス活性を示す ERK もこの場合アポトーシス促進に働く。細胞周期を制御する CDK2，p21 蛋白質や，アポトーシス促進因子である omi もシスプラチンによるアポトーシスメカニズムに重要とされる。シスプラチンは細胞内の活性酸素の生成も誘導し，この経路からも細胞死に寄与していると考えられている。小胞体もまたシスプラチン毒性の細胞内標的オルガネラであり，小胞体ストレス誘導によるアポトーシスにかかわっている[12]。

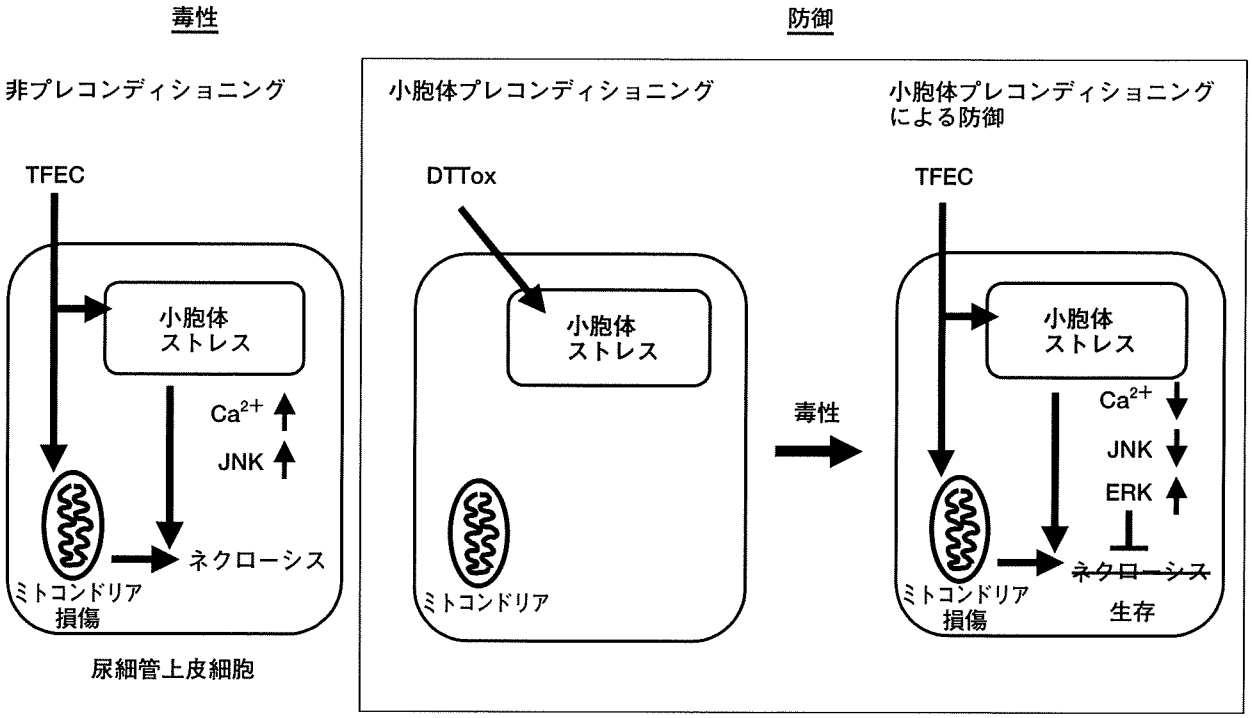

図3　小胞体プレコンディショニングによる細胞の毒物からの防御

IV. 細胞毒に対する防御能と細胞内シグナリングによる活性化

細胞は多様な細胞毒に対する防御能を備えており，それら発現を制御するシグナリング系が存在する。人為的にそれらのシグナリング系を活性化することによって毒性の発現や進行を阻害することができる。ここではいかにして防御するか，防御能獲得の方法について動物実験による研究成果を中心にまとめる。

防御の第1に，細胞毒取り込みの抑制があげられる。ゲンタマイシン誘発腎障害における受容体メガリンに対する競合が[13]，またシスプラチン腎症には，シスプラチンの細胞内取り込みを媒介するOCT2の阻害などの方法が検討されている[14]。次に，細胞内での毒性阻害，シスプラチンを例にとれば，カスパーゼの阻害，Bcl2の活性化，MAPキナーゼの阻害などがあげられる[12]。ゲンタマイシン毒性に対するプロスタサイクリンの防御能も知られている[15]。他方，細胞障害からの修復の促進も細胞毒性に対する防御機構の1つとしてあげられており，成長因子を中心に研究が行われている[1]。

最後にわれわれが行っている小胞体プレコンディショニングの研究について防御能獲得の方法の例として紹介する（**図3**）。われわれは腎毒性のあるシステインコンジュゲートTFECが小胞体ストレスを誘導し，小胞体シャペロンであるGRP78が発現することを発見した。そしてGRP78発現の阻害は細胞の感受性を高めることを確認した[16]。小胞体ストレスは本来，ストレス応答のメカニズム，防御反応であるため，穏やかな小胞体ストレスをあらかじめ誘導させることで，プレコンディショニングを起こし，致死量の細胞毒刺激に対する防御能獲得を実現した[16~18]。このメカニズムは，細胞内カルシウム濃度，ERKの活性化，JNK阻害であることが一部わかっている[6]。この小胞体プレコンディショニングはラットを使った動物実験でも再現できることが示されている[19]。

まとめ

抗生物質や細胞毒による細胞死は，細胞内シグナリングによって制御されている。この細胞内シグナリングにはさまざまなレベルがあり，最終的に細胞死を引き起こす。そして毒性による細胞死の細胞内シグナリングを理解することは，細胞毒性による細胞死に対する防御戦略を考えるうえで重要性が高い。

文　献

1) Servais H, Ortiz A, Devuyst O, et al：Renal cell apoptosis induced by nephrotoxic drugs：cellular and molecular mechanisms and potential approaches to modulation. Apoptosis **13**：11-32, 2008
2) van de Water B, de Graauw M, Le Devedec S, et al：Cellular stress responses and molecular mechanisms of nephrotoxicity. Toxicol Lett **162**：83-93, 2006
3) Degterev A, Yuan J：Expansion and evolution of cell death programmes. Nat Rev Mol Cell Biol **9**：378-390, 2008
4) Junttila MR, Li SP, Westermarck J：Phosphatase-mediated crosstalk between MAPK signaling pathways in the regulation of cell survival. Faseb J **22**：954-965, 2008
5) Golstein P, Kroemer G：Cell death by necrosis：towards a molecular definition. Trends Biochem Sci **32**：37-43, 2007
6) Hung CC, Ichimura T, Stevens JL, et al：Protection of renal epithelial cells against oxidative injury by endoplasmic reticulum stress preconditioning is mediated by ERK1/2 activation. J Biol Chem **278**：29317-29326, 2003
7) Kitamura M：Endoplasmic reticulum stress and unfolded protein response in renal pathophysiology：Janus faces. Am J Physiol Renal Physiol **295**：F323-334, 2008
8) Periyasamy-Thandavan S, Jiang M, Wei Q, et al：Autophagy is cytoprotective during cisplatin injury of renal proximal tubular cells. Kidney Int **74**：631-640, 2008
9) Yang C, Kaushal V, Shah SV, et al：Autophagy is associated with apoptosis in cisplatin injury to renal tubular epithelial cells. Am J Physiol Renal Physiol **294**：F777-787, 2008
10) Yonezawa A, Masuda S, Nishihara K, et al：Association between tubular toxicity of cisplatin and expression of organic cation transporter rOCT2 (Slc22a2) in the rat. Biochem Pharmacol **70**：1823-1831, 2005
11) Yokoo S, Yonezawa A, Masuda S, et al：Differential contribution of organic cation transporters, OCT2 and MATE1, in platinum agent-induced nephrotoxicity. Biochem Pharmacol **74**：477-487, 2007
12) Pabla N, Dong Z：Cisplatin nephrotoxicity：mechanisms and renoprotective strategies. Kidney Int **73**：994-1007, 2008
13) Nagai J, Saito M, Adachi Y, et al：Inhibition of gentamicin binding to rat renal brush-border membrane by megalin ligands and basic peptides. J Control Release **112**：43-50, 2006
14) Tanihara Y, Masuda S, Katsura T, et al：Protective effect of concomitant administration of imatinib on cisplatin-induced nephrotoxicity focusing on renal organic cation transporter OCT2. Biochem Pharmacology 2009, doi：10. 1016/j. bcp. 2009. 06. 014
15) Hsu YH, Chen CH, Hou CC, et al：Prostacyclin protects renal tubular cells from gentamicin-induced apoptosis via a PPARalpha-dependent pathway. Kidney Int **73**：578-587, 2008
16) Liu H, Bowes RC 3rd, van de Water B, et al：Endoplasmic reticulum chaperones GRP78 and calreticulin prevent oxidative stress, Ca^{2+}disturbances, and cell death in renal epithelial cells. J Biol Chem **272**：21751-21759, 1997
17) Halleck MM, Liu H, North J, et al：Reduction of trans-4,5-dihydroxy-1,2-dithiane by cellular oxidoreductases activates gadd153/chop and grp78 transcription and induces cellular tolerance in kidney epithelial cells. J Biol Chem **272**：21760-21766, 1997
18) Liu H, Miller E, van de Water B, et al：Endoplasmic reticulum stress proteins block oxidant-induced Ca^{2+} increases and cell death. J Biol Chem **273**：12858-12862, 1998
19) Asmellash S, Stevens JL, Ichimura T：Modulating the endoplasmic reticulum stress response with trans-4,5-dihydroxy-1,2-dithiane prevents chemically induced renal injury *in vivo*. Toxicol Sci **88**：576-584, 2005

*　　*　　*

Biochemical Pharmacology 77 (2009) 1429–1436

Contents lists available at ScienceDirect

Biochemical Pharmacology

journal homepage: www.elsevier.com/locate/biochempharm

Transport of guanidine compounds by human organic cation transporters, hOCT1 and hOCT2

Naoko Kimura, Satohiro Masuda, Toshiya Katsura, Ken-ichi Inui *

Department of Pharmacy, Kyoto University Hospital, Faculty of Medicine, Kyoto University, Sakyo-ku, Kyoto 606-8507, Japan

ARTICLE INFO

Article history:
Received 28 November 2008
Accepted 16 January 2009

Keywords:
Guanidine
Aminoguanidine
OCT1
OCT2
Uremic toxins
Kidney

ABSTRACT

Although some guanidine compounds were reported as superior substrates for organic cation transporter (OCT)2 than OCT1, it was unclear whether this guanidino group was an important factor in determining the specificity of hOCT1 and hOCT2. Using HEK293 cells transfected with human (h)OCT1 or hOCT2 cDNA, we assessed the role of hOCT1 and/or hOCT2 in the transport of guanidine compounds such as uremic toxins and therapeutic agents. Guanidine, creatinine and aminoguanidine more markedly inhibited the uptake of [^{14}C]tetraethylammonium (TEA) by hOCT2 than by hOCT1. [^{14}C]TEA uptake by hOCT2, but not hOCT1, was *trans*-stimulated by unlabeled guanidine, methylguanidine, creatinine, aminoguanidine and phenylguanidine. In patients with renal failure, the impairment of hOCT2 might decrease the excretion of guanidine, methylguanidine, and creatinine as uremic toxins. The uptake of aminoguanidine, a candidate for an anti-diabetic agent, was enhanced by hOCT2 with the Michaelis constant (K_m) of 4.10 ± 0.35 mM. Metformin, which was also an anti-diabetic agent, and creatinine more potently inhibited the uptake of [^{14}C]aminoguanidine by hOCT2 than that by hOCT1. Aminoguanidine had little impact on the uptake of [^{14}C]metformin by hOCT1, but inhibited that by hOCT2 with the IC_{50} of 1.49 ± 0.14 mM. These results indicated that the specificity of hOCT1 and hOCT2 was not determined simply by guanidino group. Among guanidine compounds, aminoguanidine was identified as a new superior substrate for hOCT2.

1. Introduction

Organic cation transporters (OCTs) play an important role in the tissue distribution of a wide variety of positively charged molecules, including drugs and endogenous substrates. Human organic cation transporter 1 (hOCT1) is preferentially expressed in the liver, and mediates hepatic uptake of cationic compounds [1,2]. In contrast, hOCT2 is specifically expressed in the renal proximal tubules, and is considered to mediate the renal uptake of cationic compounds [3,4]. Functional studies suggested that these transporters were often similar in substrate specificity [4,5], but in recent years, the compounds with a guanidino group such as guanidine, creatinine, and metformin were reported to be better substrates for OCT2 than OCT1 in rat and/or human [6–8]. However, it was unclear whether a guanidino group was important in determining the affinity of the two transporters.

Some guanidine compounds have been known as uremic toxins [9–14]. Other guanidine compounds have been reported as anti-diabetic agents, in particular, aminoguanidine is positively charged at physiological pH, and its renal clearance was more than twice the glomerular filtration rate (GFR), suggesting the contribution of tubular secretion [15–17].

The aim of this study was to compare the specificity of hOCT1 and hOCT2 for several guanidine compounds, including uremic toxins and aminoguanidine (Fig. 1).

2. Materials and methods

2.1. Materials

[Ethyl-1-^{14}C]tetraethylammonium bromide (55 mCi/mmol) was purchased from American Radiolabeled Chemicals (St. Louis, MO, USA). [^{14}C]aminoguanidine (51 mCi/mmol) and [biguanidine-^{14}C]metformin hydrochloride (26 mCi/mmol) were purchased from Moravek Biochemicals, Inc. (Brea, CA). [^{3}H]1-methyl-4-phenylpyridium acetate (MPP) (2.7 TBq/mmol) was purchased from PerkinElmer Life and Analytical Sciences Waltham, MA). Creatinine and guanidine hydrochloride were obtained from Nacalai Tesque (Kyoto, Japan). N_{α}-Acetyl-L-arginine, aminoguanidine bicarbonate salt, 1-butylguanidine sulfate, creatine anhydrous, 1,1-dimethylguanidine sulfate salt, guanidinoacetic acid, guanidinosuccinic acid, guanidinovaleric acid hemihydrate, methylguanidine hydrochloride, N-propylguanidine sulfate, phenylguanidine carbonate salt, 1,1,3,3-tetramethylguanidine, and 1-

* Corresponding author. Tel.: +81 75 751 3577; fax: +81 75 751 4207.
E-mail address: inui@kuhp.kyoto-u.ac.jp (K.-i. Inui).

0006-2952/$ – see front matter © 2009 Elsevier Inc. All rights reserved.
doi:10.1016/j.bcp.2009.01.010

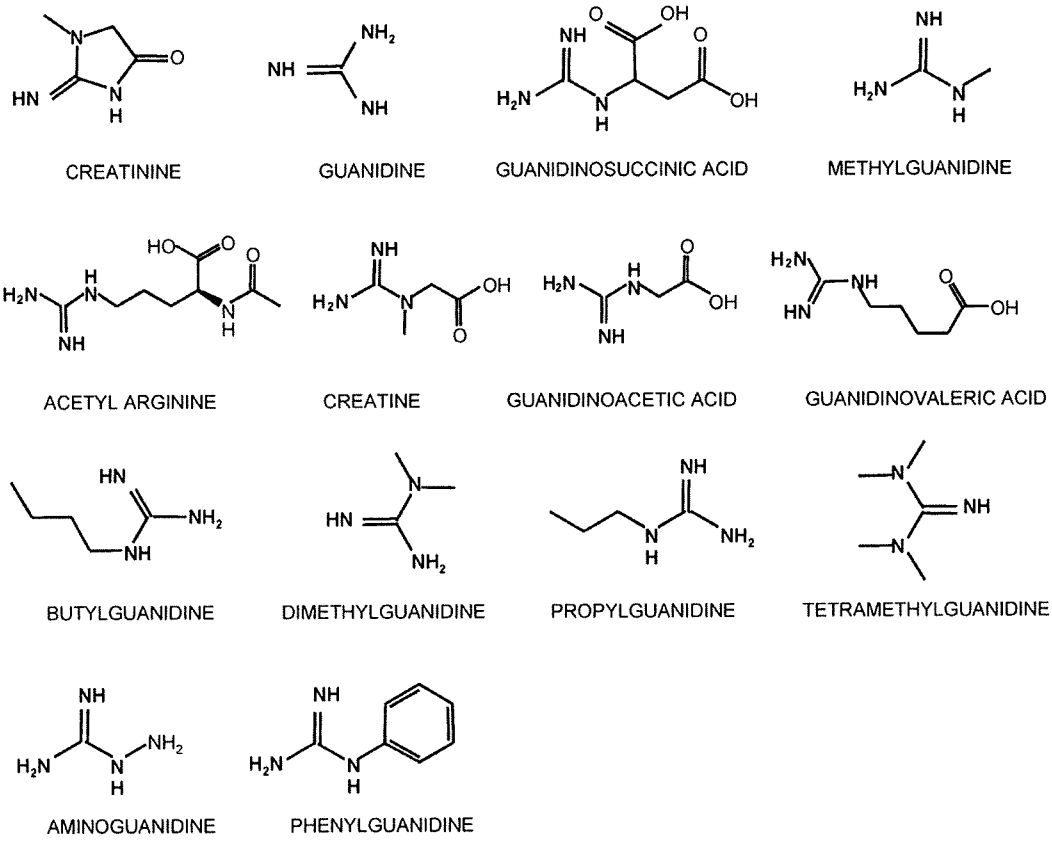

Fig. 1. Chemical structures of guanidine compounds.

methyl-4-phenylpyridium iodide were purchased from Sigma–Aldrich Co. (St. Louis, MO, USA). All other compounds used were of the highest purity available.

2.2. Cell culture

HEK 293 cells (ATCC CRL-1573, American Type Culture Collection, Manassas, VA) were cultured in complete medium consisting of Dulbecco's modified Eagle's medium with 10% fetal bovine serum in an atmosphere of 5% CO_2/95% air at 37 °C, and used as host cells. The transfectant stably expressing hOCT1 and hOCT2 were established as described previously [7,8]. The HEK293 cells transiently transfected with pCMV6-XL4 plasmid vector DNA (OriGene Technologies, Rockville, MD) containing hOCT1, hOCT2 or hOCT3-cDNA were prepared as described previously [7,18]. The cell monolayers were used at day 3 of culture for uptake experiments. In the present study, cells were used between the 78th and 90th passages.

2.3. Uptake experiments

The cellular uptake of cationic compounds was measured with monolayer cultures of HEK293 cells grown on poly-D-lysine-coated 24-well plates [7,19]. The protein content of the solubilized cells was determined by the method of Bradford [20], using a Bio-Rad Protein Assay Kit (Bio-Rad Laboratories, Hercules, CA) with bovine-globulin as a standard. For the *cis*-inhibition study, the uptake of [^{14}C]tetraethylammonium (TEA), [^{14}C]aminoguanidine, or [^{14}C]metformin was achieved by adding various concentrations of unlabeled inhibitors to the incubation medium. IC_{50} values were calculated from the inhibition plots based on the equation, $V = V_0/[1 + ([I]/IC_{50})^n]$, by a nonlinear least square regression analysis with Kaleidagraph Version 4.00 (Synergy Software, Reading, PA, USA). V and V_0 were the uptake rates of [^{14}C]TEA, [^{14}C]aminoguanidine, or [^{14}C]metformin in the presence and absence of inhibitor, respectively. [I] is the concentration of inhibitor, and n is the Hill coefficient. For the

Table 1
The apparent IC_{50} values of guanidine compounds for [^{14}C]TEA uptake by hOCT1 and hOCT2.

Guanidine compounds	IC_{50} values for [^{14}C]TEA uptake (mM)	
	hOCT1	hOCT2
Uremic toxins[a]		
Creatinine	N/A	6.06 ± 0.98
Guanidine	N/A	3.03 ± 0.42
Guanidinosuccinic acid	1.54 ± 0.15	1.47 ± 0.20
Methylguanidine	2.36 ± 0.06	1.53 ± 0.31
Acetyl arginine	N/A	N/A
Creatine	N/A	N/A
Guanidinoacetic acid	N/A	N/A
Guanidinovaleric acid	0.66 ± 0.03	1.18 ± 0.14*
Butylguanidine	0.21 ± 0.02	0.12 ± 0.01*
Dimethylguanidine	0.54 ± 0.09	0.36 ± 0.02
Propylguanidine	0.36 ± 0.04	0.29 ± 0.02
Tetramethylguanidine	0.48 ± 0.08	0.78 ± 0.13
Aminoguanidine	N/A	0.80 ± 0.11
Phenylguanidine	0.23 ± 0.03	0.26 ± 0.02

See experimental conditions in the legend of Fig. 2. The apparent IC_{50} values were calculated from inhibition plots (Fig. 2) by nonlinear regression analysis as described in Section 2. The data represent the mean ± S.E. of three independent experiments. N/A, not available. *$P < 0.05$, significantly different from the IC_{50} value of hOCT1.

[a] [18].

trans-inhibition study, the cells were preincubated with either the incubation medium (control) or the incubation medium plus the indicated concentration of unlabeled compounds for 30 min. The cells were rinsed twice with 1 mL of ice-cold incubation medium before the uptake experiments. The concentration dependence of the transport of aminoguanidine by hOCT1 and hOCT2 was analyzed using the Michaelis–Menten equation; $V = V_{max}\cdot[S]/(K_m + [S]) + K_{diff}\cdot[S]$, where V is the transport rate, V_{max} is the maximum transport rate, [S] is the concentration of aminoguanidine, K_m is the Michaelis constant and K_{diff} is a diffusion constant. The accumulation of [^{14}C]aminoguanidine by hOCT1- and hOCT2-HEK293 cells was measured at various concentrations (0.1–10 mM) for 2 min at 37 °C (pH 7.4).

2.4. Statistical analysis

Data were expressed as the mean ± S.E. Data were analyzed statistically using the non-paired Student's *t* test or one-way analysis of variance (ANOVA) and Dunnett's multiple comparison procedure.

3. Results

3.1. Inhibitory effects of guanidine compounds on TEA uptake by hOCT1 and hOCT2

To compare the specificity of hOCT1 and hOCT2, the inhibitory effects of several guanidine compounds on the uptake of [^{14}C]TEA

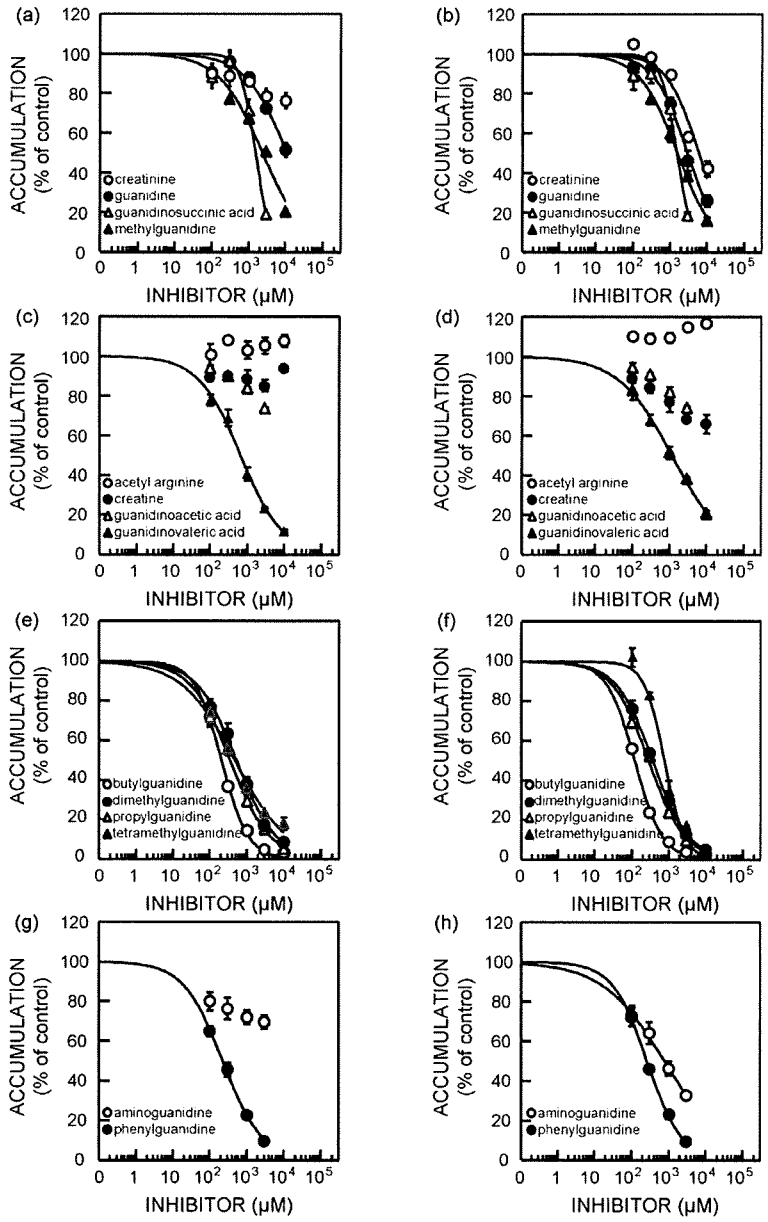

Fig. 2. Effects of guanidine compounds on [^{14}C]TEA uptake by hOCT1 (a, c, e and g) and hOCT2 (b, d, f and h). HEK293 cells transfected with hOCT1 and hOCT2 were incubated at 37 °C for 2 min with 5 μM [^{14}C]TEA (pH 7.4) in the presence of (a and b); creatinine (open circle), guanidine (closed circle), guanidinosuccinic acid (open triangle), or methylguanidine (closed triangle), (c and d); acetyl arginine (open circle), creatine (closed circle), guanidinoacetic acid (open triangle), or guanidinovaleric acid (closed triangle), (e and f); butylguanidine (open circle), dimethylguanidine (closed circle), propylguanidine (open triangle), or tetramethylguanidine (closed triangle), (g and h); aminoguanidine (open circle), or phenylguanidine (closed circle). Each point represents the mean ± S.E. of three independent experiments.

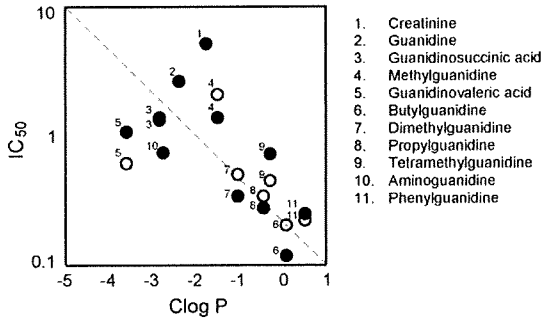

Fig. 3. Relationship between the calculated hydrophobicity (*C* log *P*) of guanidine compounds and IC_{50} values for inhibition of [^{14}C]TEA uptake by hOCT1 and hOCT2. The relationship between the calculated hydrophobicity (*C* log *P*) of guanidine compounds and the measured IC_{50} values for inhibition of [^{14}C]TEA uptake in hOCT1-HEK293 (open circle) and hOCT2-HEK293 (closed circle) cells. See experimental conditions in the legend of Fig. 2. The apparent IC_{50} values were calculated from inhibition plots (Fig. 2) by nonlinear regression analysis as described in Section 2. Octanol/water partition coefficients (log *P*) were calculated using Chem Draw Ultra 7.0 software.

(a typical substrate for the organic cation transporter) were examined (Table 1, Fig. 2). The inhibitory effects of guanidinosuccinic acid and methylguanidine were comparable between hOCT1 and hOCT2. Guanidine and creatinine had stronger inhibitory effects on [^{14}C]TEA uptake by hOCT2 than by hOCT1, whereas guanidinovaleric acid inhibited hOCT1 more than hOCT2. Guanidinoacetic acid tended to inhibit the uptake of [^{14}C]TEA by both hOCT1 and hOCT2, while creatine tended only to inhibit the hOCT2. Acetyl arginine did not inhibit [^{14}C]TEA uptake by either transporters. The inhibition curves of alkyl guanidine compounds for [^{14}C]TEA uptake showed that alkyl guanidine compounds had potent inhibitory effects on both hOCT1 and hOCT2, and that only butylguanidine had moderately higher affinity for hOCT2 than hOCT1. Phenylguanidine had an inhibitory effect on [^{14}C]TEA uptake by both hOCT1 and hOCT2, while aminoguanidine had a much greater inhibitory effect on hOCT2 than hOCT1. Fig. 3 plots the relationship between the log of the measured IC_{50} values (Table 1) and the calculated log *P* values (*C* log *P*) of guanidine compounds.

3.2. *Trans*-stimulation effects of guanidine compounds on TEA uptake by hOCT1 and hOCT2

To examine whether these guanidine compounds were substrates of hOCT1 and hOCT2, *trans*-stimulation experiments were performed. The transfectants were preincubated with a concentration equivalent to approximately 3-fold the IC_{50} value of the unlabeled guanidine compounds, or else with 10 mM if the IC_{50} value was not available (Table 1) [5]. Then, the [^{14}C]TEA uptake by the preincubated transfectants was measured. Fig. 4 shows the

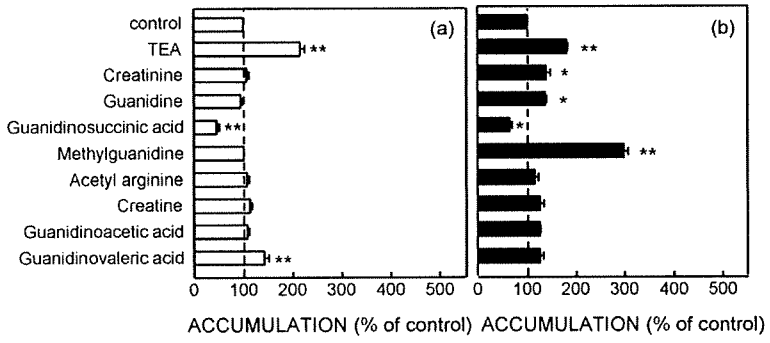

Fig. 4. *Trans*-stimulation effects of guanidine compounds as uremic toxins on [^{14}C]TEA uptake by hOCT1 (a) and hOCT2 (b). HEK-hOCT1 and HEK-hOCT2 cells were incubated for 2 min at 37 °C with 5 μM [^{14}C]TEA after preincubation with incubation medium (control) or incubation medium containing TEA (5 mM), creatinine (10 mM, hOCT1; 20 mM, hOCT2), guanidine (10 mM, hOCT1; 9 mM, hOCT2), guanidinosuccinic acid (5 mM, hOCT1; 4 mM, hOCT2), methylguanidine (7 mM hOCT1; 5 mM, hOCT2), acetyl arginine (10 mM), creatine (10 mM), guanidinoacetic acid (10 mM), and guanidinovaleric acid (2 mM, hOCT1; 4 mM, hOCT2) for 30 min at 37 °C, respectively. Data are expressed as a percentage of the control value. Control values for HEK-hOCT1 and HEK-hOCT2 were 25.6 ± 1.4 and 14.5 ± 1.2 pmol/mg protein/2 min, respectively. Each column represents the mean ± S.E. of three independent experiments. $^{*}P < 0.05$, $^{**}P < 0.01$, significantly different from the control.

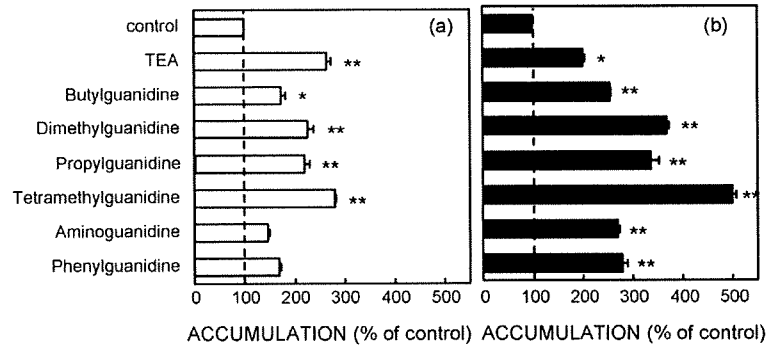

Fig. 5. *Trans*-stimulation effects of alkyl guanidine compounds, aminoguanidine and phenylguanidine on [^{14}C]TEA uptake by hOCT1 (a) and hOCT2 (b). HEK-hOCT1 and HEK-hOCT2 cells were incubated for 2 min at 37 °C with 5 μM [^{14}C]TEA after preincubation with incubation medium (control) or incubation medium containing TEA (5 mM), butylguanidine (0.6 mM, hOCT1; 0.4 mM, hOCT2), dimethylguanidine (2 mM hOCT1; 1 mM, hOCT2), propylguanidine (1 mM, hOCT1; 0.9 mM, hOCT2), tetramethylguanidine (1 mM, hOCT1; 2 mM, hOCT2), aminoguanidine (10 mM, hOCT1; 2 mM hOCT2) and phenylguanidine (0.7 mM, hOCT1; 0.8 mM, hOCT2) for 30 min at 37 °C, respectively. Data are expressed as a percentage of the control value. Control values for HEK-hOCT1 and HEK-hOCT2 were 25.9 ± 1.4 and 11.0 ± 0.2 pmol/mg protein/2 min, respectively. Each column represents the mean ± S.E. of three independent experiments. $^{*}P < 0.05$, $^{**}P < 0.01$, significantly different from the control.

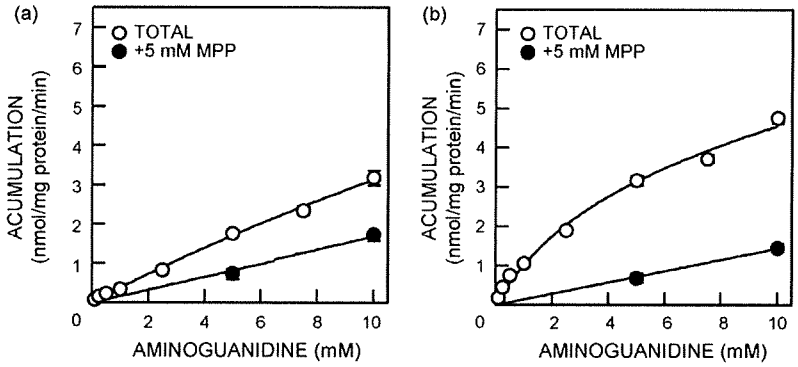

Fig. 6. Concentration dependence of [^{14}C]aminoguanidine transport by hOCT1 (a) and hOCT2 (b). hOCT1 and hOCT2 transfectants were incubated at 37 °C for 2 min with various concentrations of [^{14}C]aminoguanidine (0.1, 0.25, 0.5, 1, 2.5, 5, 7.5 and 10 mM) in the absence (open circle) or presence (closed circle) of 5 mM 1-methyl-4-phenylpyridinium (pH 7.4). Each point represents the mean ± S.E. of three independent experiments.

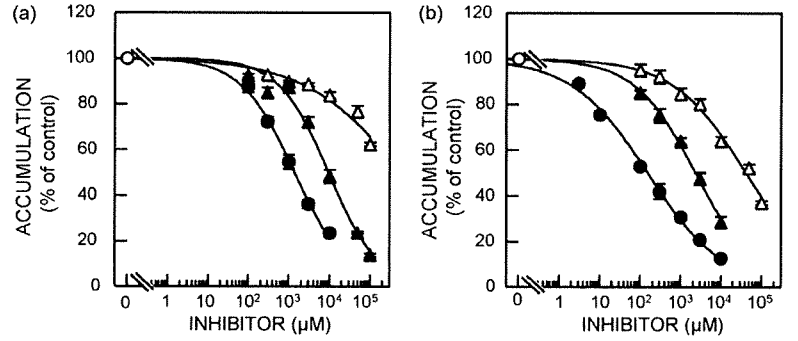

Fig. 7. Effects of TEA, creatinine and metformin on [^{14}C]aminoguanidine transport by hOCT1 (a) and hOCT2 (b). HEK 293 cells transfected with hOCT1 and hOCT2 were incubated at 37 °C for 2 min with 10 μM [^{14}C]aminoguanidine (pH 7.4) in the absence (open circle) or presence of TEA (closed circle), creatinine (open triangle), or metformin (closed triangle). Each point represents the mean ± S.E. of three independent experiments.

trans-stimulation effects of endogenous guanidine compounds as uremic toxin. Preincubation with unlabeled guanidine, methylguanidine, and creatinine significantly increased the uptake of [^{14}C]TEA by hOCT2 but not hOCT1. Meanwhile, preincubation with guanidinovaleric acid increased the [^{14}C]TEA uptake by hOCT1 but not hOCT2. As shown in Fig. 5, we examined the *trans*-stimulation effects of the other guanidine compounds. Preincubation with unlabeled butylguanidine, propylguanidine, dimethylguanidine, and tetramethylguanidine increased the uptake of [^{14}C]TEA by both transfectants. On the other hand, the preincubation with aminoguanidine and phenylguanidine significantly enhanced the [^{14}C]TEA uptake by hOCT2 but not hOCT1.

3.3. Uptake of aminoguanidine by hOCT1 and hOCT2

To obtain more information about the substrate specificity of hOCT2, the transport characteristics of [^{14}C]aminoguanidine was compared between hOCT1 and hOCT2. Fig. 6 shows the concentration dependence of [^{14}C]aminoguanidine uptake by hOCT1 and hOCT2. The uptake by hOCT2 was greater than that by hOCT1. The uptake was saturated at high concentrations in hOCT2-expressing cells, although no such saturation was observed in hOCT1-expressing cells. The apparent Michaelis–Menten constant (K_m) for the uptake of [^{14}C]aminoguanidine by hOCT2 was 4.10 ± 0.35 mM. The maximal uptake rate (V_{max}) in hOCT2-expressing cells was 4.40 ± 0.42 nmol/mg protein/min (mean ± S.E. of three separate experiments). Next, we examined the inhibitory effects of TEA, creatinine and metformin on the uptake of [^{14}C]aminoguanidine by hOCT1 and hOCT2 (Fig. 7). Fig. 7a and b shows the inhibition curves of TEA, creatinine and metformin in hOCT1- and hOCT2-expressing cells, respectively. Although TEA, creatinine and metformin inhibited the uptake of [^{14}C]aminoguanidine by both hOCT1 and hOCT2 in a dose-dependent manner, the uptake by hOCT2 was more inhibited. We calculated the IC_{50} values of these cationic compounds from the inhibition plots as described in Section 2 (Table 2). We also examined the inhibitory effect of aminoguanidine on the uptake of [^{14}C]metformin (Fig. 8). Aminoguanidine had little impact on the uptake of [^{14}C]metformin by hOCT1, and the IC_{50} value of aminoguanidine was not estimated (Fig. 8a). However, aminoguanidine inhibited the [^{14}C]metformin uptake by hOCT2 with the IC_{50} of 1.49 ± 0.14 mM (Fig. 8b).

To confirm aminoguanidine as a new substrate selective for hOCT2, the influence of *cis*-inhibition and *trans*-stimulation of aminoguanidine on the [^{3}H]MPP transport by hOCT3 was

Table 2
The apparent IC_{50} values of cationic compounds for [^{14}C]aminoguanidine uptake by hOCT1 and hOCT2.

Inhibitors	IC_{50} values for [^{14}C]aminoguanidine uptake (mM)	
	hOCT1	hOCT2
TEA	1.39 ± 0.06	0.16 ± 0.02
Creatinine	N/A	42.4 ± 2.6
Metformine	9.48 ± 0.56	2.37 ± 0.20

See experimental conditions in the legend of Fig. 7. The apparent IC_{50} values were calculated from inhibition plots (Fig. 7) by nonlinear regression analysis as described in Section 2. The data represent the mean ± S.E. of three independent experiments. N/A, not available.